Scilight

Regenerative Medicine and Dentistry
https://www.sciltp.com/journals/rmd

Review

Check for updates

Topographical Regulation of Macrophage-Mediated Osteoimmunomodulation for Bone Regeneration

Wen-Jia Han [1], Yu-Qing Mu [2,3,4], Jia-Wei Xing [1], Bo-Wen Zheng [1], Yao Liu [1], En Luo [1,*] and Ze He [1,2,3,4,*]

[1] State Key Laboratory of Oral Diseases & National Center for Stomatology & National Clinical Research Center for Oral Diseases, West China Hospital of Stomatology, Sichuan University, Chengdu 610041, China
[2] School of Medicine and Dentistry, Griffith University, Gold Coast Campus, Southport QLD 4222, Australia
[3] Institute for Biomedicine and Glycomics, Griffith University, Southport QLD 4222, Australia
[4] Australian Centre for Precision Health and Technology, Griffith University, Southport QLD 4222, Australia
* Correspondence: luoen521125@sina.com (E.L.); heze.scn@foxmail.com (Z.H.)

How To Cite: Han, W.-J.; Mu, Y.-Q.; Xing, J.-W.; et al. Topographical Regulation of Macrophage-Mediated Osteoimmunomodulation for Bone Regeneration. *Regenerative Medicine and Dentistry* **2026**, *3*(2), 8. https://doi.org/10.53941/rmd.2026.100008

Received: 26 March 2026
Revised: 14 May 2026
Accepted: 22 May 2026
Published: 5 June 2026

Abstract: The immune response plays a critical role in determining the fate of bone biomaterials, with macrophages serving as central orchestrators of the osteoimmune network. Topographical features have emerged as a powerful physical cue that can modulate macrophage function independent of biochemical signals, offering a stable and controllable strategy for immunomodulation in bone regeneration. This review systematically summarizes recent advances in understanding how topographical features regulate macrophage behavior and the underlying mechanotransduction mechanisms. We first discuss the role of macrophages in bone homeostasis, highlighting their functional plasticity and dynamic polarization during the healing process. We then provide an overview of micro- and nanofabrication techniques for constructing topographical features on biomaterial surfaces, including top-down approaches such as photolithography, etching, as well as bottom-up strategies like electrospinning and self-assembly. Subsequently, we examine the effects of topography on key macrophage behaviors and functions, including adhesion, migration, proliferation, polarization, and phagocytosis. We further dissect the molecular mechanisms by which cells sense and transduce topographical signals, focusing on integrin-mediated focal adhesion, cytoskeletal remodeling, nuclear mechanotransduction, and downstream signaling pathways, including YAP/TAZ, MRTF-A, RhoA/ROCK, and PI3K-AKT-mTOR. Emerging evidence on epigenetic regulation by topographical cues is also discussed. Finally, we present future perspectives on dynamic topography, machine learning-assisted high-throughput screening, the modulation of macrophage subtypes, and the integration of bactericidal and immunomodulatory functions. By bridging materials science and immunology, this review aims to provide a theoretical foundation for the rational design of next-generation immunomodulatory biomaterials for bone regeneration.

Keywords: topographical cues; macrophage; osteoimmunology; bone regeneration

1. Introduction

Bone tissue defects often result from trauma, tumors, infections, and other factors. In clinical practice, these defects are primarily treated through approaches such as autologous bone grafting, allogeneic bone transplantation, and distraction osteogenesis [1,2]. However, these methods have limitations, including limited bone supply, risk of immune rejection, and prolonged healing time, making it difficult to meet the urgent clinical demand for efficient bone

regeneration strategies [3,4]. In recent years, significant progress has been made in the field of biomaterials for bone regeneration, offering new possibilities for bone repair. Although various bone substitute materials, such as polymers, metals, and bioceramics, have been developed [5–7], relying solely on the osteoconductive properties of these materials often falls short of achieving ideal repair in complex bone defects. A key challenge lies in designing materials that can effectively regulate cellular behavior and promote tissue regeneration.

Notably, as exogenous implants, biomaterials first trigger an immune response upon implantation [8]. This response not only affects the early host reaction to the material but also influences the activity of local osteoblasts, osteoclasts, and mesenchymal stem cells, ultimately determining the *in vivo* fate and osteogenic outcome of the material [9]. Consequently, the immune response has become a critical factor in evaluating the osteogenic potential of bone biomaterials, and material design strategies have gradually shifted from pursuing "bio-inertness" to incorporating "immunomodulatory functions" [9]. Among the various targets of immune regulation, macrophages, as key effector cells of innate immunity, can polarize into pro-inflammatory M1 phenotypes and pro-reparative M2 phenotypes. Through the secretion of cytokines, they directly or indirectly regulate the activity of osteogenesis-related cells, playing a pivotal role in the process of bone regeneration [10,11]. Therefore, designing materials that can modulate the immune function of macrophages to mediate osteogenesis has become an important research direction in bone tissue engineering.

Surface topography of materials refers to the geometric features of the morphology and structure of a biomaterial surface, primarily involving surface shape, texture, protrusions and pits, and porosity [12]. Topographical features can be macroscale porous scaffold structures [13], or microscale protrusions, pores, grooves, or texture structures [14–16]. These topographical features determine the surface physicochemical properties of the material, such as hydrophilicity, roughness, and tensile strength [17]. More importantly, they influence cell adhesion, spreading, migration, proliferation, and differentiation by affecting the interactions between cells and the material interface [18]. With advances in micro- and nanofabrication technologies, researchers can now precisely construct topographical features with specific scales and arrangements, such as nanotube arrays and aligned fiber networks [19,20]. These structures provide new perspectives for understanding how topographical features are perceived and transduced by cells. In the field of bone tissue engineering, the design of surface topography is evolving from passive scaffolds toward active immunomodulatory platforms, which aim to shape a pro-regenerative microenvironment by guiding immune cell behavior [21,22].

This review systematically summarizes research progress in three interconnected areas: macrophage-mediated bone immunity, fabrication of topographical features on biomaterial surfaces, and regulation of macrophage immune responses by topographical features. Macrophage biology and its role in bone homeostasis are first introduced, covering their functional plasticity, regulation of bone resorption and formation, and dynamic polarization during bone healing. Fabrication strategies for topographical features are then summarized, including top-down fabrication methods and bottom-up fabrication methods. The core of the review systematically discusses how topography regulates macrophage behaviors, namely adhesion, migration, proliferation, phagocytosis, and polarization, organized by feature scale, temporal dynamics, and general trends and controversies. Mechanotransduction pathways linking topographical cues to macrophage responses are subsequently outlined. Finally, concluding remarks and future perspectives are presented.

2. Macrophages and the Osteoimmune Network

2.1. Functional Plasticity of Macrophages

The skeletal and immune systems are closely interconnected, forming an "osteoimmune network" in which bone cells, immune cells, and their secreted cytokines collectively regulate bone remodeling, repair, and homeostasis [23]. Within this network, macrophages serve as central effector cells of the innate immune system, distinguished by their remarkable functional plasticity [24]. Macrophages can polarize into distinct functional states in response to microenvironmental cues, enabling them to flexibly adapt to tissue homeostasis, injury repair, and pathological challenges [25]. M1 (classically activated) macrophages, induced by lipopolysaccharide, interferon-γ, or tumor necrosis factor-α (TNF-α), highly express inducible nitric oxide synthase (iNOS) and secrete pro-inflammatory cytokines such as interleukin-1β (IL-1β), IL-6, and TNF-α. Their primary functions include pathogen clearance, immune response initiation, and tissue debris removal [26,27]. In contrast, M2 (alternatively activated) macrophages, induced by IL-4, IL-10, or IL-13, highly express arginase-1 (Arg-1), CD206, and CD163, and secrete pro-reparative factors including IL-10, transforming growth factor-β (TGF-β), and bone morphogenetic protein-2 (BMP-2), contributing to inflammation resolution, angiogenesis, and tissue remodeling [28]. In recent years, the further subdivision of M2 subtypes has gained attention: M2a, induced by IL-4 or IL-13, primarily exhibits anti-inflammatory effects and promotes bone regeneration [29]; M2b possesses both pro- and anti-

inflammatory properties and highly expresses TNF-α and CCL1 [30]; M2c has anti-inflammatory properties similar to M2a but reaches peak expression much earlier [31]; M2d, induced by adenosine or IL-6, is involved in immunosuppression and angiogenesis, though its role in fracture healing remains controversial [31].

2.2. Macrophages Regulate Bone Homeostasis

Macrophages regulate bone resorption through multiple pathways. On one hand, macrophages serve as precursors of osteoclasts and, upon stimulation with macrophage colony-stimulating factor (M-CSF) and receptor activator of nuclear factor-κB ligand (RANKL), differentiate into mature osteoclasts [32,33]. Binding of RANKL to its receptor RANK on osteoclast precursors activates NF-κB and MAPK signaling pathways via TRAF6, ultimately inducing the expression of NFATc1, a master transcription factor for osteoclast differentiation [34]. M-CSF, through its receptor c-Fms, not only promotes the proliferation and survival of osteoclast precursors but also upregulates RANK expression, thereby facilitating RANKL function [35,36].

On the other hand, macrophages indirectly regulate osteoclast formation and activity by secreting various cytokines. TNF-α secreted by M1 macrophages is one of the most potent osteoclastogenic factors, directly promoting osteoclast precursor differentiation and synergistically enhancing RANKL-induced osteoclastogenesis through activation of the NF-κB and PI3K/Akt signaling pathways [37,38]. IL-1 mediates TNF-α-induced RANKL expression and enhances osteoclastogenesis in the presence of RANKL [39]. IL-6 upregulates the expression of osteoclast-related genes such as NFATc1, ACP5, and CTSK through the JAK2/STAT3 signaling pathway, thereby promoting osteoclast formation [40]. Conversely, anti-inflammatory cytokines secreted by M2 macrophages, including IL-4, IL-10, and IL-13, inhibit osteoclast formation. IL-4 and IL-13 downregulate RANKL expression and upregulate osteoprotegerin (OPG) via STAT6-dependent signaling pathways [41]. OPG, acting as a decoy receptor for RANKL, competitively blocks the interaction between RANKL and RANK, thus negatively regulating bone resorption [42]. IL-10 suppresses osteoclastogenesis by inhibiting the expression of c-Fos and c-Jun, thereby downregulating NFATc1 expression [43].

Beyond regulating bone resorption, macrophages play an indispensable role in supporting bone formation. A classic study by Chang et al. demonstrated that macrophage depletion significantly inhibits osteoblast-mediated bone formation *in vivo*, highlighting the necessity of macrophages for the osteogenic process [44]. *In vitro* co-culture experiments further confirmed that macrophages significantly enhance the osteogenic differentiation capacity of bone marrow mesenchymal stem cells and mouse pre-osteoblasts, an effect dependent on the polarization state of the macrophages [22].

M2 macrophages play a dominant role in promoting bone formation. They secrete multiple factors such as BMP-2, TGF-β, oncostatin M (OSM), IL-10, and IL-4, which promote osteogenic differentiation through distinct signaling pathways. BMP-2 activates the PI3K/AKT signaling pathway, significantly enhancing the impaired osteogenic function of BMSCs under diabetic conditions and upregulating the expression of alkaline phosphatase (ALP), osteocalcin (OCN), and osteopontin (OPN) to drive osteogenic differentiation [45,46]. OSM activates the STAT3 signaling pathway, inducing osteogenic differentiation of BMSCs while inhibiting their adipogenic differentiation [47,48]. IL-10 enhances the osteogenic capacity of periosteum-derived stem cells (PDSCs) via the JAK1-STAT3 pathway [49]. As a classic pro-osteogenic factor, TGF-β not only promotes the expression of Runx2 and ALP through Smad proteins but has also recently been shown to upregulate the expression of Periostin, a key factor mediating angiogenesis-osteogenesis coupling [50]. Furthermore, IL-4-activated M2 macrophages exhibit elevated TGF-β1 expression, which subsequently activates the TGF-β1/Smad signaling pathway in BMSCs to promote their osteogenic differentiation [51].

In contrast, M1 macrophages primarily exert negative regulatory effects on osteogenic differentiation. TNF-α inhibits the expression of key osteogenic factors, including IGF-1 and RUNX2, thereby suppressing osteogenic differentiation. It should be noted that the effect of TNF-α on osteoblasts remains somewhat controversial, with some studies suggesting that at low levels, it may also possess certain osteogenic potential [52]. IL-6 inhibits the Wnt-β-catenin pathway by upregulating DKK-1 and SOST, thereby suppressing osteogenic differentiation. The Wnt-β-catenin pathway is a key signaling axis that promotes RUNX2 expression and osteoblast differentiation [53].

2.3. Dynamic Polarization of Macrophages

Bone healing progresses through inflammation, bone formation, and remodeling phases, each requiring distinct macrophage phenotypes [31]. During the early stage of healing, M1 macrophages dominate the local microenvironment. They obtain energy through enhanced glycolysis, rapidly clear pathogens and necrotic tissue debris, and secrete pro-inflammatory factors such as IL-6 and TNF-α to initiate the immune response [54]. Simultaneously, M1 macrophages recruit mesenchymal stem cells (MSCs) and endothelial progenitor cells by

secreting CCL2 and vascular endothelial growth factor (VEGF), laying the cellular foundation for subsequent repair [55] Transient and moderate M1 signaling can also activate early osteogenic transcriptional programs in MSCs through the COX-2/PGE2 pathway [56,57], indicating that a controlled inflammatory phase is necessary for initiating bone repair [58]. As inflammation subsides, macrophage metabolism shifts from glycolysis to oxidative phosphorylation (OXPHOS) [59], driving the transition from the M1 to the M2 phenotype. M2 macrophages promote inflammation resolution by secreting anti-inflammatory factors such as TGF-β and IL-10, while also recruiting pericytes to stabilize blood vessels and promote vascular maturation through platelet-derived growth factor (PDGF) [60,61]. They further promote osteogenic differentiation and inhibit osteoclast activity to maintain the balance between bone resorption and formation. Timely transition from M1 to M2 phenotype is essential for successful bone regeneration. Persistent M1 polarization leads to chronic inflammation, inhibiting osteoblast activity and promoting fibrous encapsulation [62]. Conversely, premature M2 polarization may also lead to excessive fibrosis, impairing implant integration, highlighting the critical importance of precise temporal control over macrophage polarization [63].

In summary, macrophages serve as central coordinators of the osteoimmune network, orchestrating the balance between bone resorption and formation through the dynamic transition of their polarization states. M1 and M2 macrophages, via their characteristic cytokine secretion profiles, primarily drive bone resorption and bone formation, respectively, and their sequential balance determines the outcome of bone regeneration. A deep understanding of this regulatory network not only elucidates the physiological basis of bone homeostasis maintenance but also provides a theoretical foundation for designing bone repair materials with active immunomodulatory functions. The pivotal role of macrophages in orchestrating bone homeostasis and repair is summarized in Figure 1.

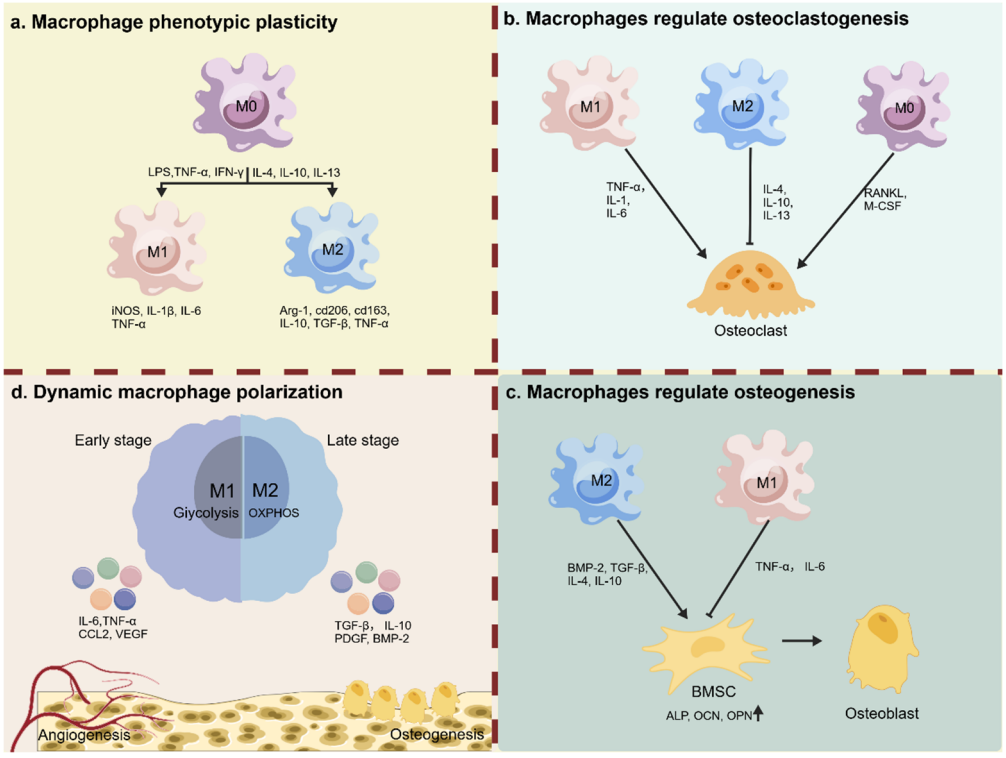

Figure 1. Macrophage Polarization and Its Role in Bone Homeostasis and Repair. (**a**) M0 macrophages polarize into M1 (LPS/TNF-α/IFN-γ) or M2 (IL-4/IL-10/IL-13), characterized by iNOS/IL-1β/IL-6/TNF-α and Arg-1/CD206/CD163/IL-10/TGF-β/TNF-α, respectively. (**b**) M1 macrophages secrete TNF-α/IL-1/IL-6 to promote osteoclastogenesis via RANKL/M-CSF, while M2 macrophages produce IL-4/IL-10/IL-13 to suppress it. (**c**) M1 macrophages inhibit osteoblast differentiation via TNF-α/IL-6, whereas M2 macrophages promote BMSC differentiation into osteoblasts via BMP-2/TGF-β/IL-4/IL-10. (**d**) The coordinated actions of both early M1 and late M2 phases collectively promote bone formation and angiogenesis. Created with BioGDP [64].

3. Methods for Constructing Topographical Features on Biomaterials

The construction of topographical features relies on advancements in micro- and nanofabrication technologies, which can be broadly classified into top-down and bottom-up strategies. Top-down approaches achieve precise

structural fabrication by processing or modifying the surface of existing bulk materials; bottom-up approaches generally refer to the process of constructing topographical features through the ordered stacking, assembly, or growth of atoms, molecules, or macroscopic material units. By selecting different methods and parameters based on the material properties and application requirements, precise control over the topography can be achieved.

3.1. Top-Down Fabrication Methods

Top-down methods start from macroscopic materials and construct topographical features by removing, reshaping, or modifying the material surface. Photolithography is one of the most mature techniques, using a photomask and photoresist to form micron-scale patterns on substrates such as silicon wafers, which can serve as master molds for subsequent replication [65,66]. Soft lithography primarily uses elastomers, mainly polydimethylsiloxane (PDMS), as stamp or mold materials to efficiently fabricate micron-scale topographical features via replica molding. By casting uncured PDMS onto the surface of a photolithographically fabricated silicon master mold and peeling it off after thermal curing, a PDMS stamp or mold with complementary micron-scale topography can be obtained [67]. Biela et al. utilized soft lithography to prepare PDMS substrates with groove widths of 2–10 μm and depths of 50–200 nm by varying the parameters of the photolithographic master mold [68]. Inspired by spider web structures, Wu et al. employed a template replication method to construct double-sided centripetal microgroove topographies on poly(D,L-lactide-co-caprolactone) (PLCL) films. They first fabricated PDMS stamps with complementary structures using a micropatterned silicon master, then imprinted the stamps onto both sides of the PLCL film at 190 °C, precisely replicating the centripetal radial microgroove array [69].

Traditional microcontact printing typically uses the raised features of a stamp to pick up an "ink" and then stamp it to form patterns. However, this method faces challenges such as difficulty in thickness control, significant residue, and limited substrate adaptability. To address these limitations, Joo et al. developed an intaglio contact printing method. This method utilizes the recessed features of a PDMS stamp as a template, fills them with a carbon nanotube/paraffin composite, and after solidification, transfers the entire structure onto the target substrate. This technique enables high-resolution pattern fabrication (<10 μm), allows precise control over pattern thickness by adjusting the groove depth, and can be transferred onto various substrates, including glass, metal, paper, polymers, and even human skin [70]. Nanoimprint lithography achieves high-precision pattern replication by pressing a hard mold with nanoscale surface relief features into a polymer resist. It offers resolutions below 10 nm, simple processing, and low cost. Based on the curing mechanism, it is divided into thermal nanoimprint lithography and ultraviolet nanoimprint lithography. The former utilizes the glass transition of thermoplastic polymers, while the latter uses UV curing of liquid precursors at room temperature [71,72]. Building upon this, Sansen et al. developed soft nanoimprint lithography, combining laser interference lithography with sol-gel chemistry to fabricate silica nanopillar arrays with tunable diameters of 400–850 nm and controllable heights on glass substrates. These were used to study the mechanical response of cell membranes to nanotopography and the spatial organization of membrane proteins [73].

Etching is a subtractive pattern transfer technique that involves removing material from specific areas. Based on the etching mechanism, it can be divided into wet etching and dry etching. Wet etching uses chemical reagents such as acids or bases for material removal, offering low cost and high material selectivity [74]. Ariganello et al. oxidized titanium surfaces with an H_2SO_4/H_2O_2 mixed solution for 2 h, forming a uniform mesoporous network with pore sizes of 20–22 nm and depths of 10–20 nm [75]. Odegaard et al. used hydrofluoric acid (HF) chemical etching for post-treatment of Ti6Al4V alloy surfaces fabricated by electron beam melting (EBM). Through a two-step process (0.5% HF solution, 4 min each), they effectively removed unmelted particles, reduced surface roughness, and introduced a fluoride-modified layer, thereby influencing the adhesion and differentiation behavior of osteoblasts [76]. Dry etching refers to a material removal process performed in a vacuum chamber using gaseous plasma, where etching is achieved through physical sputtering, chemical reactions, or a combination of both. The primary advantage of dry etching over other etching methods is its ability to achieve anisotropy [77]. Seong et al. fabricated silicon nanoneedle arrays with tunable tip diameters (20–700 nm) and a height of 5 μm using a combination of deep reactive ion etching (DRIE) and reactive ion etching (RIE) sharpening processes. DRIE achieves anisotropic deep etching through alternating etching and passivation steps, while RIE sharpens the nanopillar tips via isotropic etching, enabling precise control over the tip curvature [78]. Roy et al. employed maskless oxygen plasma reactive ion etching to fabricate high-aspect-ratio nanopillar and nanowire arrays on polyethylene terephthalate (PET) surfaces. By adjusting parameters such as radio frequency power, gas flow rate, and chamber pressure, they could control the morphology and dimensions of the nanostructures. The resulting nanostructures exhibited a cooperative stiffening effect induced by capillary forces, endowing the flexible polymer substrate with mechanobactericidal activity [79].

Laser processing utilizes the thermal and photochemical effects of lasers to form micro- and sub-microstructures on material surfaces. For example, femtosecond lasers can create patterned micropores on decellularized vascular grafts, causing minimal thermal damage to the tissue, enabling precise control over pore size and spacing, with pore depths reaching up to 200 μm and fully penetrating the graft's middle layer [80]. Sandblasting is a common industrial method for surface roughening. By controlling parameters such as particle size, impact velocity, and surface coverage, different roughness levels can be achieved on metal surfaces. Valverde et al. systematically studied the effect of alumina sandblasting parameters on titanium surface roughness, finding that the highest surface roughness values (Sa ≈ 2.6 μm, Sdr ≈ 4 μm) were obtained with a particle size of 100 μm, impact velocity of 100 m/s, and surface coverage of 5 g/in^2 [81].

Electrochemical anodization can grow TiO_2 nanotube arrays in situ on metals like titanium. The nanotube diameter can be precisely controlled by adjusting the anodization voltage [82]. Wang et al. anodized titanium sheets in an electrolyte containing HF and H_3PO_4 at voltages of 5 V and 20 V for 1.5 h, followed by sintering at 450 °C for 3 h, obtaining TiO_2 nanotube arrays with diameters of approximately 30 nm and 100 nm, respectively [83]. Hydrothermal methods can be used to construct sheet array structures with identical chemical composition but tunable dimensions on titanium surfaces. Zheng et al. successfully prepared magnesium-aluminum layered double hydroxide sheet array surfaces with sheet sizes of approximately 74.5 nm, 0.85 μm, and mixed nano/micro scales by controlling the hydrothermal reaction conditions [84].

Thermoplastic forming technology is suitable for special materials like bulk metallic glasses. Shayan et al. successfully fabricated nanorod arrays with a diameter of 55 nm by imprinting an anodized aluminum oxide template onto a Pt-based bulk metallic glass surface via hot embossing [85]. The needle-punching method achieves physical forming of existing fibrous materials through mechanical entanglement. The Fabric-16 polyglycolic acid nonwoven scaffold used by Horii et al. was prepared by needle-punching, forming a dual-region structure of "fiber bundles" and "holes" with a fiber bundle spacing of approximately 5.0 μm and a hole spacing of approximately 825.4 μm, thereby constructing a topographical morphology with hierarchical porosity [86].

3.2. Bottom-Up Fabrication Methods

Bottom-up methods construct topographical features through the assembly of molecules or nanoscale units. Electrospinning is the most widely used technique for fabricating fibrous topographies. It uses a high-voltage electric field to stretch a polymer solution into continuous fibers. By adjusting the collection device, either disordered or aligned fiber networks can be obtained. Jiang et al. prepared poly(L-lactic acid) (PLLA) nanofiber membranes with aligned (2500 rpm) or random (10 rpm) orientations by controlling the rotation speed of the electrospinning collector [87]. The preparation of hydrogel fibers via electrospinning can be achieved through two strategies: simultaneous crosslinking and post-crosslinking. Simultaneous crosslinking involves placing a UV light source at the spinneret to initiate free radical polymerization of the extruded monomers during jetting. Post-crosslinking involves first fabricating a fibrous scaffold via electrospinning, followed by inducing molecular crosslinking within the fibers through photopolymerization or metal chelation to form a hydrogel [88]. Melt blowing is a continuous fiber assembly technique that uses high-temperature airflow to draw molten polymer and a rotating drum for collection, enabling the ordered stacking of micro/nanofibers and the construction of three-dimensional network structures. Horii et al. used melt blowing to prepare polyglycolic acid nonwoven scaffolds (Fabric-0.9, Fabric-3), achieving precise control over fiber diameter and pore structure by adjusting process parameters such as extrusion temperature, air temperature, and collection distance [86]. Building on fibrous scaffolds, solution-induced crystallization can further create nanoscale topographies. Zhu et al. immersed a PCL fiber scaffold in a 0.5% PCL/amyl acetate solution for 40 min. At room temperature, this induced the ordered crystallization of PCL molecular chains on the fiber surface, forming nanoscale "shish-kebab" structures, resulting in fiber scaffolds with varying pore sizes and surface roughness [89]. Electrospinning can also be combined with other techniques for functional design. Zhang et al., building on electrospun radially aligned PCL bilayer fiber membranes, further incorporated coaxial electrospray to deposit EGF-loaded collagen nanoparticles onto the fiber surface. By using a dynamic aperture to create a particle density gradient increasing from the periphery to the center, they successfully integrated topographical physical signals with biochemical signals [90].

Layer-by-layer assembly enables the construction of multilayer structures with precisely controlled composition and architecture. Asadi Tokmedash et al. alternately deposited MXene nanosheets and hydroxyapatite onto a pre-stretched polystyrene substrate using layer-by-layer assembly, followed by heat-induced shrinkage to create wrinkles. This successfully generated nano- to micro-scale wrinkled topographies with wavelengths of 372–2010 nm and amplitudes of 193–979 nm, allowing continuous adjustment of feature size by controlling the number of assembled layers [91]. Microfluidics enables the controllable fabrication of nanomaterial topographies through

precise control of multi-channel flow rates. Ye et al. used a PDMS microfluidic chip to regulate the flow rates of cysteine (10–120 μL·min^{-1}) and gold nanorods (20–100 μL·min^{-1}), achieving a series of morphological evolutions from conformal growth to multi-spiked structures. This approach offers advantages over traditional batch synthesis, including lower reagent consumption, higher mixing efficiency, and continuous production capability [92]. Colloidal self-assembly represents another versatile bottom-up strategy for generating ordered topographical features. In this approach, monodisperse colloidal nanoparticles or microspheres spontaneously arrange into close-packed arrays (e.g., hexagonal close-packed structures) via capillary forces, electrostatic interactions, or solvent evaporation. These assemblies can serve as masks for etching or as templates for inverse opal structures, enabling precise control over feature size (from tens of nanometers to several micrometers) and geometry (pits, pillars, honeycombs) across large areas [93].

Physical templating offers new avenues for constructing three-dimensional topographical features. Directional freezing induces the oriented growth of ice crystals by controlling the freezing temperature; combined with in situ photocrosslinking, it produces porous scaffolds with continuous radial channels. Wang et al. used a GelMA/SilMA/HAp precursor solution, induced radial ice crystal growth at −30 °C, and then performed UV photocrosslinking to fix the structure, obtaining radially microchanneled scaffolds with uniform and interconnected pores [94]. Advances in extrusion-based 3D printing have further expanded the ability to construct cross-scale topographies. Wu et al. systematically reviewed three improved extrusion-based 3D printing strategies: cryogenic-assisted extrusion, which uses ice crystals as natural porogens to create micron-scale pores within the filaments; sacrificial template/particle leaching extrusion, which introduces soluble particles that are dissolved post-printing to create internal micropores; and particle-sintered extrusion, which generates micron-scale surface textures on the printed filaments through high-temperature sintering. These innovations enable the fabrication of scaffolds with centimeter-millimeter-micrometer tri-scale structures, better mimicking the hierarchical architecture of natural bone [95]. Aboal-Castro et al. used melt-extrusion 3D printing to construct macroporous polycaprolactone (PCL) scaffolds. After each layer was printed, a femtosecond laser was used to etch the fiber surface, creating parallel microgrooves (10 μm and 80 μm wide) and micropits (25 μm in diameter). This process did not compromise the scaffold's mechanical properties, and the 10 μm wide microgrooves significantly enhanced human mesenchymal stem cell adhesion and induced cell alignment along the groove direction [96].

4. Topographical Regulation of Macrophage Behaviors and Functions

The interaction between biomaterial topographical features and macrophages is a critical determinant of implant success and bone regeneration. Topographical features influence virtually every aspect of macrophage behavior, from adhesion and migration to proliferation, phagocytosis, and ultimately phenotypic polarization, collectively determining whether the implant induces a pro-inflammatory (M1) or pro-healing/osteogenic (M2) microenvironment. The key topographical parameters (geometry, orderliness, and scale) that govern these macrophage responses are schematically summarized in Figure 2.

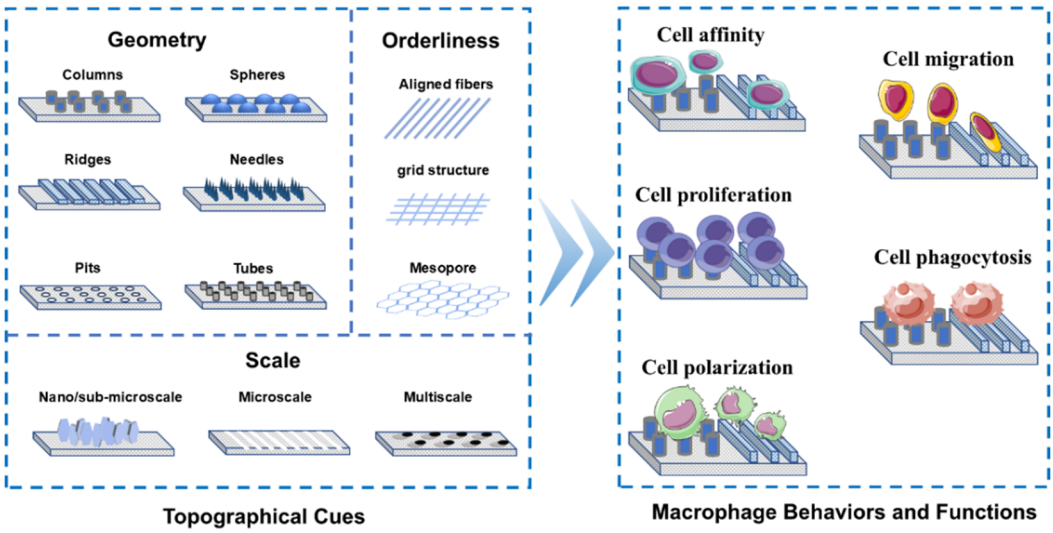

Figure 2. Regulation of Macrophage Behaviors and Functions by Material Surface Topographical Cues. This figure systematically summarizes the core topographical parameters of biomaterial surfaces that regulate macrophage

responses, and the corresponding cellular biological effects. The left panel concludes three key dimensions determining the immunomodulatory effects of topography: geometry, dimensional scale, and structural orderliness. The right panel shows the core behaviors (adhesion, proliferation, migration, phagocytosis) and functional phenotypes (M1/M2 polarization) of macrophages mediated by topographical cues via regulating cell adhesion and morphological remodeling.

4.1. Regulation of Macrophage Behavior by Topographical Features

Topographical features can be sensed by cells and translated into biological responses, thereby regulating cell fate [84]. For macrophages, topographical features on material surfaces can influence their multiple behaviors independent of chemical cues, including adhesion, migration, proliferation, polarization, and phagocytosis. These behavioral changes ultimately determine their immunomodulatory function during bone regeneration [97].

4.1.1. Regulation of Macrophage Adhesion by Topographical Features

Cell adhesion is the initial event in the interaction between macrophages and materials, and also serves as the foundation for subsequent immune responses. Topographical features significantly influence the adhesion strength of macrophages by altering the effective contact area and geometric constraints of the material surface. Compared with microscale scaffolds, nanoscale scaffolds provide a higher specific surface area and thus offer more abundant integrin-binding sites, which is more conducive to cell adhesion in tissue engineering [98]. Macrophages cultured on nanosheet array surfaces (with sheet edge length of approximately 74.5 nm) exhibited a spindle-like morphology with short, thick pseudopodia. The expression of adhesion-related genes, integrin β2 and focal adhesion kinase (FAK), was significantly higher than on microsheet surfaces or titanium surfaces, indicating that topography at this scale facilitates integrin clustering and focal adhesion formation [84]. The scale of physical topography also influences macrophage spreading behavior. Zhu et al. found that 90 nm TiO_2 honeycomb structures promoted the formation of abundant pseudopodia in macrophages, significantly increasing their spreading area. In contrast, 5 μm structures restricted pseudopodia formation, causing cells to adopt an "embedded" state with limited spreading [10]. Furthermore, the high specific surface area of oriented structures further enhances cell adhesion [98]. The topography of oriented microfibers can guide the directional migration of macrophages along the fiber axis. Acting as "pioneer cells", macrophages are the first to establish a directionally aligned cellular network on the fiber surface, providing a physical guidance template for the subsequent migration of Schwann cells and axonal regeneration [99]. Surface chirality can also indirectly influence macrophage adhesion by regulating protein adsorption. He et al. demonstrated that chiral gold nanoarrays (L-300 and D-300) modulate macrophage adhesion by affecting the adsorption amount and conformation of fibronectin (FN). Molecular dynamics simulations revealed that the D-chiral surface exhibits higher affinity for FN, forming more hydrogen bonds and having a larger contact area, thereby enhancing macrophage adhesion [100].

4.1.2. Regulation of Macrophage Migration by Topographical Features

Cell migration is notably guided by topographical features. The classic phenomenon of contact guidance also exists in macrophages, with cells tending to align and directionally migrate along anisotropic topographical structures [101,102]. Wójciak-Stothard et al. investigated the effect of micron-scale grooves on the behavior of macrophage-like cells (P388D1 cell line). They found that the patterned substrate significantly activated cell spreading and elongation, and markedly increased the persistence and speed of cell movement [103]. Further studies indicate that nanoscale topographical structures also regulate macrophage migration. Real-time tracking using transparent titanium films revealed that the migration distance (average 720 μm) and speed (1.0 μm/min) of macrophages on nanorough surfaces (RMS ≈ 4.76 nm) were significantly lower than those on flat surfaces (850 μm, 1.3 μm/min). This was accompanied by reduced FAK phosphorylation and fewer actin stress fibers [104]. Beyond scale differences, the specific morphological features of topography also affect macrophage migration. Studies show that when cells are cultured on nanoscale ridge-and-groove structures, they tend to migrate towards the ridge structures rather than into the grooves [105]. Patterned micropores created on decellularized vascular grafts using femtosecond laser significantly promoted macrophage migration and infiltration into the material interior. When the micropore spacing was controlled below 250 μm, cells nearly completely occupied the middle layer of the material within two weeks post-implantation [80].

4.1.3. Regulation of Macrophage Proliferation by Topographical Features

Local proliferation of macrophages is an important pathway for maintaining immune cell numbers and is significant for constructing the immune microenvironment around implants. The dimensions of nanotopography significantly affect macrophage proliferation. After 72 h of culture on 10–100 nm nanopatterned dot arrays, the number of macrophages increased by 10.6% to 149.1% compared to smooth surfaces. The increase was most pronounced on surfaces with 50 nm features (149.1%), while the number of cells on 200 nm surfaces decreased by 41.2%. Combined with changes in cell spreading area and the expression of adhesion-related proteins, these results indicate that nanotopography with feature sizes around 50 nm provides the most suitable microenvironment for cell growth, whereas 200 nm surfaces are unfavorable for cell adhesion and growth, leading to apoptotic-like morphological changes [105]. Macrophages derived from THP-1 cells cultured on nanorough surfaces constructed with 16, 38, and 68 nm gold nanoparticles showed a significant increase in cell number over time (from Day 1 to Day 7), indicating that nanotopography supports long-term cell adhesion and proliferation [106]. The spacing between nanotubes also influences macrophage proliferation. After 72 h of culture on TiO_2 nanotube surfaces with 20 nm and 80 nm spacing, the number of RAW 264.7 cells was reduced compared to flat titanium surfaces. This effect was more pronounced under inflammatory conditions induced by LPS. Notably, under these conditions, the cell proliferation rate was higher on surfaces with 80 nm spacing than on those with 20 nm spacing, suggesting that a larger tube spacing may be more favorable for maintaining macrophage survival in an inflammatory microenvironment [107].

4.1.4. Regulation of Macrophage Phagocytosis by Topographical Features

Different surface topographies significantly influence the phagocytic function of macrophages. Nano-micro hybrid wrinkled topographies can enhance the phagocytic capacity of macrophages. On surfaces pre-attached with bacteria, macrophages exhibited more pronounced pseudopodia extension, and the residual biofilm coverage for Staphylococcus aureus and Escherichia coli decreased to 8.05% and 13.3% of the control group (without macrophages), respectively. Notably, this surface endowed macrophages with context-dependent immunomodulatory capabilities. In a sterile environment, macrophages polarized toward the anti-inflammatory M2 phenotype (with upregulated CD206 and IL-10 expression) and secreted osteoinductive factors such as BMP-2 to promote tissue repair. In the presence of bacteria, however, macrophages enhanced their pro-inflammatory M1 response and phagocytic function, effectively clearing pathogens [108]. Micron-scale topography also affects phagocytic function. Cicuendez et al. encapsulated RAW 264.7 macrophages in porcine decellularized adipose matrix hydrogels with different pore sizes (HG5, ~0.07 μm; HG10, ~0.04 μm) while keeping the biochemical composition and mechanical properties comparable. They found that macrophages encapsulated in the larger-pore hydrogel (HG5) exhibited significantly higher phagocytosis of Candida albicans than those in the smaller-pore hydrogel (HG10) [109]. Beyond pore size, the specific geometry of micron-scale topographies also dictates phagocytic efficiency. Macrophages cultured on microgroove/ridge surfaces phagocytosed significantly more particles (15.19 particles per cell) than those cultured on micropillar surfaces (10.89 particles per cell) [110]. Nanotopography further enhances phagocytic function. On nanostructured zirconia surfaces with a roughness of 9–27 nm, the phagocytic rate of THP-1 macrophages increased from approximately 50% to 80%, and the phagocytic index also increased significantly. This enhancement is attributed to actin reorganization. Although polymerized actin used for adhesion was reduced on the rough surface, actin repolymerized during phagocytosis, supporting the formation of phagocytic cups and particle internalization [111].

4.2. Topographical Regulation of Macrophage Polarization

The structures of cells, such as integrins, focal adhesions, and filopodia, are all in the range of tens to hundreds of nanometers, and they can only “sense” physical topographies with dimensions similar to their own [112,113]. Therefore, the “scale” of topographical features is the primary factor determining whether it can be perceived by cells and trigger subsequent signaling cascades [114]. Accordingly, this section is organized by feature scale to systematically elucidate the effects of distinct topographical parameters, namely, geometry, orderliness, on macrophage polarization and osteogenic outcomes. Representative studies on topography-mediated macrophage polarization are summarized in Table 1.

Table 1. Representative topographical features regulating macrophage polarization and related biological effects.

Topographical Scale	Material	Topographical Features	Cell Type	Biological Effects	Reference
Nano/sub-microscale	AuNPs + pOX coating	AuNP-induced nano-roughness (16/38/68 nm AuNP diameter; corresponding RMS roughness 3.4/10.3/16.2 nm)	PMA-differentiated THP-1 macrophages	38 nm AuNP surfaces most effectively promote M2 polarization (significantly upregulate Arginase and IL-4, downregulate TNF-α and IL-1β); 16 nm AuNP surfaces induce a transient M1 phenotype; all nano-rough surfaces time-dependently drive M2 polarization	[106]
	TiO_2/Ti	TiO_2 nanotubes (65, 92, 142 nm)	THP-1	All TiO_2 nanotube diameters promote M2 polarization (↑CD206, ARG1, IL-10; ↓CD86, IL-1β, TNF-α), with 142 nm showing the strongest effect; conditioned medium enhances HUVEC endothelialization via VEGF/ERK1/2/PI3K-AKT	[115]
	PDMS	Small nanopillars (SNPLs: 450 nm diameter, 300 nm spacing); Large nanopillars (LNPLs: 700 nm diameter, 800 nm spacing); Nanopits (NPTs: 700 nm diameter, 150 nm depth, 800 nm spacing)	RAW264.7	LNPLs exert mild pro-M2 effect (weaker than SNPLs & NPTs). SNPLs induce cell spreading, NPTs induce cell elongation. Both SNPLs and NPTs upregulate M2 markers (CD206, CD163, IL-10, IL-1ra) and downregulate M1 markers (CCR7, IL-6, IL-1β) compared with LNPLs and flat surface	[116]
	Ti	Micro-/nano-grooves (150 nm–50 μm)	Mouse BMDMs	Elongation peaks at 400–500 nm; ↑Arg1, ↑IL-10; no change in iNOS/TNF-α; promotes M2 pro-healing phenotype	[117]
	PLLA	Aligned electrospun PLLA nanofibers (~758 nm diameter) vs. random fibers	RAW264.7	Aligned fibers induce elongation, suppress M1 (↓iNOS, TNF-α, IL-1β), promote M2 (↑Arg-1, IL-4, IL-10, TGF-β) via JAK-STAT & NF-κB; CM promotes fibroblast/collagen/angiogenesis; *in vivo* accelerates wound healing, reduces M1, increases M2	[118]
Microscale	β-TCP ceramic	Unidirectional microgrooves (0, 25, 50, 75 μm spacing)	RAW264.7	75 μm groove spacing maximizes M2 polarization (↑CD206, ↓CCR7) and osteoinductive factors (BMP-2, OSM); CM enhances BMSC osteogenesis	[119]
	BCP ceramic	BCP whiskers: solid long (7–10 μm) vs. hollow short (2–3 μm)	RAW264.7	Short hollow (BCP HW) promotes elongation, M2, ↑BMP-2/TGF-β1; solid long (BCP W) induces M1; CM enhances osteogenesis via BMP/Smad & TGF-β/Smad	[120]
	PCL	Melt-electrowritten PCL scaffolds: box-, triangle-, round-, disordered; box-shaped pores 40–100 μm	Primary human macrophages	Box geometry most pro-M2; 40 μm pores best promote elongation, ↑CD163, CD206, IL-10; larger pores (≥80 μm) reduce M2 markers	[121]
	Polystyrene	TopoChip micropatterns (3–23 μm diameter, 10 μm height) from circles/triangles/rectangles	Human CD14+ monocyte-derived macrophages	Cylindrical micropillars dominate attachment vs. other shapes; 5–10 μm pillars drive highest attachment; combination of pillar size & density determines M1→M2 shift; machine learning identifies pattern area as key predictor	[122]
Multiscale	Ti	Micropits (5–15 μm) vs. micropits + nanopores (10–25 nm)	RAW264.7	Micropits alone induce round, M1-like; micro/nano hybrid promotes spindle-shaped, M2 (↓iNOS, ↑CD206)	[123]
	PLGA/PCL/collagen	Electrospun PLGA/PCL/fish collagen core-shell fibers with micro-nano pores	RAW264.7	Hierarchical micro-nano pore structure promotes M2 polarization; enhances new bone formation (BV/TV, trabecular microarchitecture) *in vivo*	[124]
	Ti	Micro/nano net on Ti by alkali heat treatment (SAM at 60 °C vs. SAH at 90 °C)	Mouse BMDMs	SAH (larger nanopores 60–150 nm) promotes elongation & M2 more than SAM (30–100 nm); faster angiogenesis, improved bone-implant contact	[125]
	Polymer	Latticed electrospun membrane (~500 μm grid-like pores)	Host-derived macrophages (mouse/rat calvarial defect)	Recruits more macrophages; upregulates M2 genes (Arg1, Ccl2, Ccl22, Il4ra); activates HIF-1α/VEGF → enhanced angiogenesis; superior bone regeneration vs. random/aligned fibers	[126]
	Si + PMMA	Colloidal self-assembled pattern: 5 μm Si particles + 100 nm PMMA particles, hexagonal close-packed arrangement	RAW264.7, THP-1, primary human PBMC macrophages	Suppresses LPS-induced M1 polarization: ↓NO, ↓iNOS, ↓IL-6, ↓TNF-α, ↓IL-1β, ↓TLR4, ↓$CD11b^+CD86^+$; downregulates mechanosensitive gene Piezo1	[93]

4.2.1. Nano/Sub-microscale Topographies

Submicron and nanoscale topographies (1–1000 nm) can be sensed by macrophages through a combination of filopodia probing, integrin clustering, and cell-scale morphological adaptation [127,128]. Dabare et al. constructed a model with controllable surface roughness by immobilizing gold nanoparticles (AuNPs) of 16, 38, and 68 nm onto a plasma-polymerized 2-methyl-2-oxazoline (pOX) surface, followed by a 5 nm pOX overcoating to unify the surface chemistry [106]. Over time (from day 1 to day 7), the secretion of pro-inflammatory cytokines (TNF-α, IL-1β) decreased, while anti-inflammatory cytokines (Arg-1, IL-4) increased. Among them, the 38 nm roughness surface exhibited the best performance in promoting M2 polarization and suppressing M1 polarization [106]. Xu et al. fabricated TiO_2 nanotubes with diameters of ~65 nm, ~92 nm, and ~142 nm. All three nanotube diameters promoted M2 polarization and suppressed M1 markers compared to flat titanium, with the 142 nm nanotubes exhibiting the strongest anti-inflammatory effect (highest CD206, Arg-1, IL-10; lowest CD86, IL-1β, TNF-α). Conditioned media from macrophages cultured on these nanotubes enhanced HUVEC adhesion, proliferation, migration, and tube formation, effects mediated by VEGF secretion and the ERK1/2 and PI3K/AKT pathways [115]. The comparison between nanopillars and nanopits reveals geometry-dependent effects. Li et al. fabricated small nanopillars (SNPLs: 450 nm diameter, 300 nm spacing), large nanopillars (LNPLs: 700 nm, 800 nm spacing), and nanopits (NPTs: 700 nm diameter, 150 nm depth, 800 nm spacing). LNPLs induced macrophage morphologies and M1/M2 marker expression similar to the flat control. SNPLs induced spreading and NPTs induced elongation; both upregulated M2 markers (CD206, CD163, IL-10, IL-1ra) and downregulated M1 markers (CCR7, IL-6, IL-1β). Thus, both spreading and elongation drive M2 polarization, highlighting the critical role of feature geometry and spacing [116]. Beyond pillars and pits, submicron groove patterns also effectively modulate macrophage behavior. Luu et al. used titanium surfaces with precisely controlled groove widths of 400–500 nm. These submicron grooves maximally elongated macrophages and drove them toward an anti-inflammatory, pro-healing M2 phenotype, as evidenced by elevated IL-10 secretion [117]. The alignment of fibrous scaffolds similarly directs macrophage phenotype. Aligned electrospun PLLA nanofibers (~758 nm diameter) induced macrophages to elongate into a spindle shape along the fiber direction. In an LPS-induced inflammatory environment, compared to random fibers, the aligned fibers significantly suppressed M1 polarization (↓iNOS, TNF-α, IL-1β) and upregulated M2 markers (↑Arg-1, IL-4, IL-10, TGF-β) [118].

4.2.2. Microscale Topographies

When feature sizes exceed the submicron range and enter the microscale (≥1 μm), individual topographical units become too large for filopodia to grasp or for single cells to fully envelop. Consequently, macrophages respond through cell-scale morphological changes such as spreading and elongation. Hao et al. fabricated β-TCP substrates with parallel microgrooves of 0, 25, 50, and 75 μm spacing via DLP 3D printing. These grooves induced macrophages to align along the direction of the grooves, accompanied by a morphological shift from spherical to spindle-shaped. Among the tested spacings, the 75 μm grooves exhibited the most pronounced M2 polarization phenotype, with the highest expression of osteoinductive cytokines BMP-2 and OSM [119]. Wu et al. fabricated two whisker structures on biphasic calcium phosphate (BCP) ceramics: solid long whiskers (BCP-W, 7–10 μm) and hollow short whiskers (BCP-HW, 2–3 μm). BCP-HW promoted macrophage elongation, M2 polarization, and upregulated BMP-2/TGF-β1, whereas BCP-W induced M1 polarization. Conditioned medium from BCP-HW-treated macrophages enhanced MC3T3-E1 osteogenesis via BMP/Smad and TGF-β/Smad pathways, highlighting the key role of whisker geometry (length, solid/hollow) in macrophage polarization and osteoinductivity [120]. Beyond pore size, the geometry of pores also critically modulates macrophage polarization. Tylek et al. fabricated PCL-based melt-electrowritten scaffolds with four distinct pore geometries (box-shaped, triangle-shaped, round, and disordered) and found that box-shaped scaffolds most effectively promoted M2-like polarization in primary human macrophages, as evidenced by downregulation of IL-1β and IL-8 and upregulation of CD163 [121]. Vassey et al. employed a high-throughput TopoChip containing 2176 micropatterns (3–23 μm diameter, 10 μm height) generated from three primitive shapes (circles, triangles, rectangles). By screening human monocyte/macrophage responses across this diverse library, they found that cylindrical micropillars dominated cell attachment compared to other geometries such as triangular or rectangular pillars. Moreover, among micropillars, those with diameters of 5–10 μm drove the highest attachment, and the combination of pillar size and spacing determined the shift from pro-inflammatory M1 to anti-inflammatory M2 phenotypes [122].

4.2.3. Multiscale Topographies

Multiscale topographies that combine nanoscale features with microscale structures offer distinct advantages by simultaneously providing cues that target different cellular sensing mechanisms. Hang et al. compared a

micropitted titanium surface (5–15 μm pits) with a hybrid surface where nanopores (10–25 nm) were further created on the micropits. While the micropitted surface alone induced a round, M1-like morphology, the micro/nano-structured surface promoted spindle-shaped, M2-polarized macrophages with lower iNOS and higher CD206 expression [123]. Jin et al. designed an electrospun PLGA/PCL/fish collagen core-shell fibrous scaffold with a hierarchical micro-nano pore structure. The scaffold exhibited micron-scale pores between fibers (approximately 500 μm) and nanoscale pores (10–25 nm in diameter, ~50 nm in depth) on individual fiber surfaces, forming a multiscale topography. The topological scaffold promoted M2 macrophage polarization and significantly enhanced new bone formation in rat calvarial defects, with improved BV/TV and trabecular microarchitecture [124]. Yang et al. constructed a micro/nano-net on sand-blasted and acid-etched titanium by alkali-heat treatment at 60 °C (SAM) or 90 °C (SAH), forming a nanoporous network on microscale pits. SAH, with larger nanopores (60–150 nm), promoted macrophage elongation and M2 polarization more effectively than SAM (30–100 nm), and this enhanced M2 skewing translated into faster angiogenesis and improved bone-implant contact *in vivo* [125]. Another example of multiscale topography is the latticed electrospun membrane reported by Jin et al. This membrane combined nanoscale fibers with a microscale grid-like pore structure (pore size ~500 μm). Subcutaneous implantation in mice revealed that the latticed membrane recruited significantly more macrophages and upregulated M2-associated genes (Arg1, Ccl2, Ccl22, Il4ra). It also activated the HIF-1α/VEGF signaling pathway, leading to enhanced angiogenesis. In rat and mouse calvarial defect models, the latticed membrane promoted superior bone regeneration compared to random or aligned fiber membranes [126]. Multiscale topographies can also be constructed via colloidal self-assembly. Song et al. fabricated cSAPs composed of 5 μm Si particles (microscale) and 100 nm PMMA particles (nanoscale) in a hexagonal close-packed arrangement (cSAP3). This multiscale topography significantly suppressed LPS-induced M1 polarization in RAW264.7, THP-1, and primary human PBMC macrophages, as evidenced by reduced NO production, downregulated iNOS, IL-6, TNF-α, IL-1β, and TLR4, and a lower proportion of $CD11b^{+}CD86^{+}$ cells [93].

4.2.4. Temporal Dynamics of Polarization

Bone healing is a highly coordinated dynamic process in which macrophages exhibit precise temporal changes in their polarization state [31]. The inflammatory phase demands a transient M1 response to clear pathogens and recruit progenitor cells. The bone formation phase requires an M1 to M2 transition to support tissue repair and angiogenesis. The remodeling phase relies on sustained M2 activity to orchestrate matrix maturation. Thus, the timely M1 to M2 transition is critical for successful bone regeneration [129]. Topographical cues can actively regulate this temporal sequence. Shen et al. investigated TiO_2 nanotubes of different diameters (30, 70, 110 nm) under oxidative stress (300 μM H_2O_2). They found that 110 nm nanotubes activated integrin/FAK/Akt mediated MAPK (JNK/p38) and NF κB signaling, which enhanced early M1 related cytokine secretion and upregulated chemokines (SDF1, IL 8, CCL2). These chemokines recruited mesenchymal stem cells (MSCs), and in turn, the recruited MSCs promoted an M1 to M2 transition of macrophages, reducing inflammation [130]. Yin et al. used genipin crosslinked collagen/chitosan scaffolds with average pore sizes of 160 μm (Col Ch 160) and 360 μm (Col Ch 360) while maintaining comparable porosity and mechanical properties. The larger pores (360 μm) significantly accelerated the M1 to M2 transition, upregulated secretion of pro angiogenic and anti-inflammatory cytokines (TGF β, IL 10, VEGF), and enhanced tube formation and migration of human umbilical vein endothelial cells. This work establishes that microscale pore size can direct the temporal switch from inflammation to regeneration [131]. Beyond static topographies, Hong et al. engineered a magnetically responsive nanocrack system with crack widths of 50, 80, and 110 nm, to which RGD ligand-modified magnetic particles were attached via elastic PEG linkers. Upon magnetic actuation, the particles moved from deep within the cracks to shallower positions, dynamically modulating ligand exposure and crack depth. This reversible control directly regulates macrophage polarization through adhesion related pathways. Moderate cracks (80 nm) in the deep state provide poor adhesion, resulting in high iNOS expression and M1 polarization under pro inflammatory conditions. However, upon magnetic shallowing, these cracks promote strong integrin recruitment and ROCK2 activation, driving macrophages toward an anti-inflammatory M2 phenotype with high Arg 1 expression [132]. This reversible control over topographical features offers a new paradigm for mimicking the dynamic mechanical remodeling of the extracellular matrix and holds promise for guiding macrophage polarization in real time. Collectively, these examples show that both static and dynamic topographical cues can orchestrate the M1 to M2 transition. Therefore, evaluating topographical designs solely by endpoint M2/M1 ratios is insufficient; the capacity to regulate the timing of polarization transitions should be a critical design criterion.

4.2.5. General Trends and Controversies

Feature size exerts a size-dependent effect on macrophage polarization. A systematic comparison by Zhu et al. demonstrated that 90 nm TiO_2 honeycomb structures significantly promoted M2 polarization, whereas the effect weakened at 500 nm, and 1 μm and 5 μm structures were largely ineffective or even biased toward M1. The smaller the feature size, the stronger the M2 polarization, showing a clear negative correlation [10]. The correlation between nanopore diameter and macrophage polarization is not strictly linear [133]. Dabare et al. reported that 38 nm roughness promoted M2 polarization more effectively than 16 nm and 68 nm, suggesting an optimal size window rather than a strict "the smaller, the better" rule [106]. Nevertheless, the overall trend remains that nanoscale topographies (<100 nm) are superior to larger dimensions [134,135]. The optimal size varies across studies (e.g., 90 nm in Zhu et al. versus 38 nm in Dabare et al.). This may be attributed to differences in cell sources, experimental conditions, and confounding variables (e.g., material systems, stiffness, wettability, composition, degradation products) that can all independently influence polarization outcomes [136–138].

Importantly, the size effect is also constrained by geometry. The optimal feature size varies with geometry. For groove structures, Luu et al. systematically fabricated titanium surfaces with groove widths ranging from 150 nm to 50 μm and demonstrated that macrophage elongation peaked at 400–500 nm, which correlated with the highest expression of the M2 marker Arg1 and secretion of IL-10, while iNOS and TNF-α remained low across all widths. This study provides direct evidence that an intermediate groove width optimally promotes a pro-healing macrophage phenotype [117]. For pore structures, using box-shaped scaffolds with precisely controlled pore sizes from 40 to 100 μm, Tylek et al. demonstrated that 40 μm pores induced the highest degree of macrophage elongation and M2 marker expression (CD163, CD206, IL-10), while scaffolds with a 100 μm pore size diminished this effect [123].

Ordered anisotropic structures, including aligned nanofibers and unidirectional microgrooves, promote M2 polarization through contact guidance [117,118]. However, the relative importance of fiber alignment versus fiber diameter in regulating macrophage inflammatory responses remains debated. Contrary to studies highlighting the anti-inflammatory benefits of fiber alignment, Saino et al. demonstrated that fiber diameter is the dominant topological determinant of macrophage proinflammatory activation. PLLA nanofibers (~0.55 μm) significantly suppressed the secretion of proinflammatory cytokines (TNF-α, IL-1β, MIP-1α) regardless of fiber alignment, whereas microfibers (~1.5 μm) triggered a markedly stronger inflammatory response in RAW 264.7 macrophages [139].

5. Mechanisms of Topography-Driven Immunophenotypic Reprogramming

How cells perceive topographical features on biomaterial surfaces and translate them into biological responses is a core scientific question for understanding topography-regulated bone regeneration. This process primarily relies on mechanotransduction. In this process, cells sense the biophysical properties of their microenvironment through integrin-mediated adhesion sites and convert mechanical forces into biochemical signals, thereby regulating cell behavior and gene expression [140]. When cells adhere to material surfaces with specific topographies, integrins cluster to form focal adhesions and recruit adapter proteins such as talin and vinculin, which connect the extracellular matrix to the actin cytoskeleton. Consequently, the phosphorylation level of FAK changes, initiating downstream signaling pathways [113,141]. Topography directly regulates the maturation and stability of focal adhesions by influencing the clustering density and distribution of integrins, thereby determining the initial adhesion strength and signal input.

Perceived mechanical signals are transmitted to the nucleus through the cytoskeletal network. Actin polymerization and contraction generate cellular tension. Mechanosensitive ion channels such as Piezo1 convert membrane stretching into calcium-dependent signaling cascades to regulate cell function [142]. Dynamic cytoskeletal structures like podosome continuously probe the topographical features of the substrate, providing feedback that regulates cell morphology and migration [143]. Integrin αX plays a role in podosome formation and cell motility [144]. Mechanical signals must ultimately be transmitted to the nucleus to regulate gene expression. The LINC complex (composed of SUN proteins on the inner nuclear membrane and KASH proteins on the outer nuclear membrane) directly connects the cytoskeleton to the nucleoskeleton (lamins), forming a continuous physical link from the extracellular matrix to the nucleus [145].

Mechanical stimuli can regulate epigenetics. Confining macrophage spreading using micropatterning techniques can downregulate the expression of histone deacetylase 3 and increase the enrichment of the repressive epigenetic mark H3K36me2 in the promoter regions of pro-inflammatory genes. This leads to chromatin compaction and transcriptional suppression of late inflammatory genes such as IL-6 and iNOS, confirming that physical signals can regulate macrophage function through epigenetic remodeling [146]. Jia et al. further revealed that titanium nanotube (TNT) surfaces reduce macrophage actin contractility by decreasing the phosphorylation

level of myosin light chain. This promotes the nuclear translocation of the histone demethylase UTX, thereby reducing the enrichment of the repressive histone modification H3K27me3 at the Abca1 gene locus, upregulating ABCA1 expression, and inhibiting the inflammatory response [147].

As classic mechanosensitive effector molecules, the nucleocytoplasmic localization of YAP/TAZ is regulated by cytoskeletal tension. In cells with good spreading and high cytoskeletal tension, YAP/TAZ translocate to the nucleus and regulate macrophage polarization toward the M2 phenotype [148–150]. Lamin A/C-mediated nuclear mechanotransduction can control the macrophage inflammatory response. Titanium nanotubes downregulate lamin A/C expression, causing the inner nuclear membrane protein emerin to dissociate from the nuclear envelope. This inhibits actin polymerization and the nuclear translocation of the actin-dependent transcriptional coactivator MRTF-A, ultimately reducing the LPS-induced macrophage inflammatory response (downregulation of IL-6, IL-1β, and CXCL9 expression). Knockdown of lamin A/C mimics the anti-inflammatory effect of TNTs, while overexpression reverses this effect [151]. Hybrid nano-micro wrinkled topographies upregulate the expression of Rho GTPase family genes through integrin clustering and focal adhesion assembly, activating the RhoA/ROCK signaling pathway. This regulates cytoskeletal rearrangement and gene expression, ultimately promoting M2 polarization [108]. The connection between the integrin-FAK signaling axis and the PI3K-AKT-mTOR pathway is bridged by ROCK. After integrin activation, phosphorylated FAK activates ROCK, which further regulates cytoskeletal rearrangement and activates the downstream PI3K-AKT-mTOR signaling pathway. This leads to upregulated expression of the anti-inflammatory transcription factors STAT3 and STAT6, ultimately driving macrophage polarization toward the M2 phenotype [84]. The key signaling pathways involved in this process are summarized in Figure 3. In summary, macrophages perceive topographical features through integrin-mediated adhesion, which are transmitted via the cytoskeleton and integrated through multiple signaling pathways including nuclear mechanotransduction, YAP/TAZ, MRTF-A, RhoA/ROCK, and PI3K-AKT-mTOR. This cascade ultimately converts physical stimuli into immunophenotypic changes, providing a theoretical basis for the targeted regulation of macrophage function through the topological design of material surfaces.

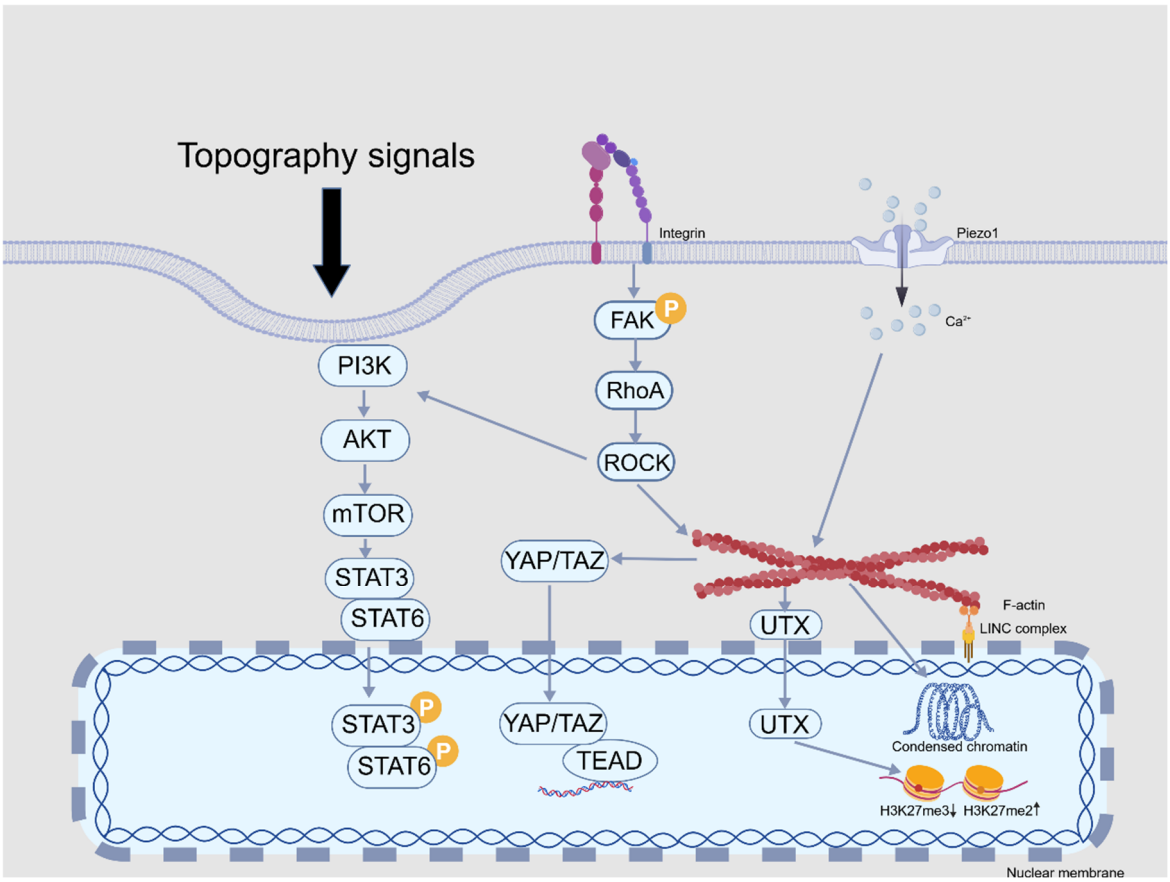

Figure 3. Mechanotransduction Pathways in Topography-Driven Macrophage Immunophenotypic Reprogramming. This diagram illustrates the cascade of molecular events through which topographical features are sensed by macrophages and translated into immunophenotypic changes. The signaling pathways involved in cytoskeletal reorganization, nuclear translocation of transcription factors, and epigenetic regulation are depicted, providing a framework for understanding how physical cues guide macrophage polarization. Created with [64].

6. Conclusions and Outlook

Osteoimmunomodulation is a key strategy in the field of bone tissue regeneration. This review systematically summarizes how topographical features on biomaterial surfaces influence the osteoimmune microenvironment and thereby intervene in the bone regeneration process by regulating the function of immune cells such as macrophages. Studies have shown that the physical parameters of topographical features (such as scale, morphology, and orderliness) can significantly affect macrophage adhesion, morphology, polarization state, and cytokine secretion, thereby playing a temporal regulatory role across the inflammatory, reparative, and remodeling phases of bone healing. Therefore, when designing next-generation bone repair biomaterials, it is essential to move beyond the traditional concept of biocompatibility and adopt "immunomodulatory capacity" as a core design criterion, actively guiding an immune microenvironment favorable for bone regeneration. Although significant progress has been made in this field, the precise molecular mechanisms by which topographical signals regulate osteoimmunity, the discrepancies between different research findings, and the translational pathway from laboratory to clinic remain largely unexplored. Future research should move beyond phenomenological description toward mechanistic deepening, technological integration, and intelligent design. Specifically, the following directions warrant focused exploration.

Machine learning enables a shift from "descriptive screening" to "mechanistic prediction". Hou et al. combined combinatorial topographic arrays fabricated by dynamic laser interference lithography with a Gaussian process regression machine learning model to achieve high-throughput screening and continuous prediction of macrophage polarization behavior. They successfully identified "hotspots" promoting M2 polarization and "coldspots" promoting M1 polarization, validating the accuracy of their predictions through scaled-up fabrication [152]. Building on this, computational prediction models can be further constructed, inputting topographical parameters and cell mechanoresponse data to predict the resulting immune response profiles. This approach can not only accelerate the design and screening of new biomaterials but also help identify key topographical feature combinations that robustly guide desired immune responses.

Furthermore, the ability of topography to regulate macrophage subtype differentiation is being increasingly explored. Carrara et al. successfully induced THP-1-derived macrophages to polarize toward the M2d subtype using 3D fractal structures with multiscale features, without adding external stimuli, as evidenced by increased IL-10 secretion and upregulated VEGF mRNA expression [153]. In the future, technologies such as single-cell RNA sequencing, proteomics, and spatial transcriptomics can be used to precisely analyze the functional status, metabolic reprogramming, and spatiotemporal distribution of different macrophage subpopulations under specific topographical stimuli, thereby revealing the deeper logic of how topography regulates the immune micro-network.

Natural structures such as cicada wing nanopillars and gecko skin spinules can destroy bacterial cell membranes through physical perforation, achieving pathogen killing [154,155]. Inspired by this, researchers have developed materials such as colloidal carbon nanotubes and graphene that kill bacteria through tip puncture or edge cutting. Surface nanopillars/spikes achieve bactericidal effects by rigidly stretching the bacterial cell membrane or storing and releasing energy through moderate elastic deformation to exacerbate membrane rupture [156,157]. Such bactericidal structures demonstrate good safety for mammalian cells, as these cells are larger and possess higher membrane elasticity, allowing them to adapt to the topological interface through deformation without rupturing [158]. Future research could explore combining bactericidal topographies with antibiotic delivery systems to construct a synergistic strategy of "physical killing + drug release" to combat implant-associated infections. Furthermore, how to integrate bactericidal and immunomodulatory functions within the same platform to achieve the dual goals of infection control and bone regeneration will be an important direction in bone tissue engineering.

It should be noted that the formation and long-term stability of surface topographies are influenced not only by fabrication methods but also by intrinsic material properties. Material stiffness affects the fidelity of micro- and nano-imprinting processes, as softer substrates may deform during demolding, compromising pattern resolution [159]. For biodegradable polymers (e.g., PLLA, PLGA), hydrolytic degradation progressively erodes surface features over time, leading to the loss of intended topographical features, as reviewed by Woodruff and Hutmacher [160]. These material-dependent changes in topographical stability may ultimately alter the persistence of physical cues that guide macrophage polarization, thereby affecting the osteoimmune microenvironment and long-term bone regeneration outcomes.

Topographical features do not act as isolated physical cues. Rather, they modulate the interfacial physicochemical environment, including protein adsorption, surface energy, wettability, ligand presentation, and local mechanical properties [161,162]. These factors collectively determine how macrophages perceive and respond to the material surface [163]. Nevertheless, multiple studies have carefully controlled surface chemistry to isolate topographical effects, demonstrating that topography alone can regulate cell behavior independent of

chemical cues [151,164]. However, the indirect contributions of these coupled variables remain important considerations when interpreting experimental outcomes and comparing across studies. Future investigations should aim to decouple topography from other material properties (e.g., stiffness, degradation, surface chemistry) to better understand their respective roles in osteoimmunomodulation.

To enhance comparability across different studies and to decouple the bidirectional interplay between topography and material-intrinsic properties (e.g., stiffness, degradation kinetics, surface chemistry, and their reciprocal modulation), future research should pursue two complementary strategies. First, standardized methods for characterizing topographical parameters and unified *in vitro* immune cell evaluation models should be established. Second, systematic comparisons across different material systems (e.g., titanium, polymers, ceramics) should be performed while keeping topographical parameters constant, thereby isolating the contribution of material-specific properties from that of topography itself, and vice versa. Such efforts will improve data reproducibility and facilitate the translation of immune-instructive biomaterials. In summary, osteoimmunomodulatory biomaterials offer a promising new paradigm for overcoming challenging bone defects. Through the deep integration of materials science, immunology, biology, and engineering, we are confident that we can design next-generation functional biomaterials that are not merely "accepted" by the body but can actively "orchestrate" efficient repair, ultimately achieving precision and intelligence in bone regeneration therapy.

Author Contributions

W.-J.H.: conceptualization, visualization, writing—original draft preparation. Y.-Q.M., J.-W.X. and B.-W.Z.: conceptualization, writing—review & editing. Y.L.: writing—review & editing, funding acquisition. E.L.: conceptualization, supervision, funding acquisition, writing—review & editing. Z.H.: conceptualization, supervision, writing—review & editing, funding acquisition. All authors have read and agreed to the published version of the manuscript.

Funding

This research was funded by National Natural Science Foundation of China [82370932, 82001016]; Program of Science and Technology Department of Sichuan Province [2024YFFK0204, 2025ZNSFSC1579, 2024NSFSC1586].

Institutional Review Board Statement

Not applicable.

Informed Consent Statement

Not applicable.

Data Availability Statement

No new data were created or analyzed in this study. Data sharing does not apply to this article.

Conflicts of Interest

The authors declare no conflict of interest.

Use of AI and AI-Assisted Technologies

No AI tools were utilized for this paper.

References

1. Wang, J.; Wu, Y.; Li, G.; et al. Engineering Large-Scale Self-Mineralizing Bone Organoids with Bone Matrix-Inspired Hydroxyapatite Hybrid Bioinks. *Adv. Mater.* **2024**, *36*, 2309875. https://doi.org/10.1002/adma.202309875.
2. Xue, N.; Ding, X.; Huang, R.; et al. Bone Tissue Engineering in the Treatment of Bone Defects. *Pharmaceuticals* **2022**, *15*, 879. https://doi.org/10.3390/ph15070879.
3. Yu, D.; Shen, W.; Dai, J.; et al. Treatment of Large Bone Defects in Load-Bearing Bone: Traditional and Novel Bone Grafts. *J. Zhejiang Univ. Sci. B* **2025**, *26*, 421–447. https://doi.org/10.1631/jzus.B2300669.
4. Sabouri, Z.; Dequeecker, M.; Anees, H.; et al. Recent Advances in Biomaterials for Bone Regeneration: Bridging Innovation and Clinical Translation. *Mater. Today Bio* **2026**, *36*, 102685. https://doi.org/10.1016/j.mtbio.2025.102685.
5. Fan, L.; Chen, S.; Yang, M.; et al. Metallic Materials for Bone Repair. *Adv. Healthc. Mater.* **2024**, *13*, 2302132. https://doi.org/10.1002/adhm.202302132.

6. Kashirina, A.; Yao, Y.; Liu, Y.; et al. Biopolymers as Bone Substitutes: A Review. *Biomater. Sci.* **2019**, *7*, 3961–3983. https://doi.org/10.1039/C9BM00664H.
7. Zhou, H.; Yang, L.; Gbureck, U.; et al. Monetite, an Important Calcium Phosphate Compound—Its Synthesis, Properties and Applications in Orthopedics. *Acta Biomater.* **2021**, *127*, 41–55. https://doi.org/10.1016/j.actbio.2021.03.050.
8. Chung, L.; Maestas, D.R.; Housseau, F.; et al. Key Players in the Immune Response to Biomaterial Scaffolds for Regenerative Medicine. *Adv. Drug Deliv. Rev.* **2017**, *114*, 184–192. https://doi.org/10.1016/j.addr.2017.07.006.
9. Chen, Z.; Klein, T.; Murray, R.Z.; et al. Osteoimmunomodulation for the Development of Advanced Bone Biomaterials. *Mater. Today* **2016**, *19*, 304–321. https://doi.org/10.1016/j.mattod.2015.11.004.
10. Zhu, Y.; Liang, H.; Liu, X.; et al. Regulation of Macrophage Polarization through Surface Topography Design to Facilitate Implant-to-Bone Osteointegration. *Sci. Adv.* **2021**, *7*, eabf6654. https://doi.org/10.1126/sciadv.abf6654.
11. Bi, Z.; Cai, Y.; Shi, X.; et al. Macrophage-Mediated Immunomodulation in Biomaterial-Assisted Bone Repair: Molecular Insights and Therapeutic Prospects. *Chem. Eng. J.* **2024**, *488*, 150631. https://doi.org/10.1016/j.cej.2024.150631.
12. Kim, E.; Tae, G. Direct Reprogramming and Biomaterials for Controlling Cell Fate. *Biomater. Res.* **2016**, *20*, 39. https://doi.org/10.1186/s40824-016-0086-y.
13. Zhang, H.; Zhang, H.; Xiong, Y.; et al. Development of Hierarchical Porous Bioceramic Scaffolds with Controlled Micro/Nano Surface Topography for Accelerating Bone Regeneration. *Mater. Sci. Eng. C* **2021**, *130*, 112437. https://doi.org/10.1016/j.msec.2021.112437.
14. Wu, S.; Shan, Z.; Xie, L.; et al. Mesopore Controls the Responses of Blood Clot-Immune Complex via Modulating Fibrin Network. *Adv. Sci.* **2022**, *9*, e2103608. https://doi.org/10.1002/advs.202103608.
15. Bartneck, M.; Schulte, V.A.; Paul, N.E.; et al. Induction of Specific Macrophage Subtypes by Defined Micro-Patterned Structures. *Acta Biomater.* **2010**, *6*, 3864–3872. https://doi.org/10.1016/j.actbio.2010.04.025.
16. Ramaswamy, Y.; Roohani, I.; No, Y.J.; et al. Nature-Inspired Topographies on Hydroxyapatite Surfaces Regulate Stem Cells Behaviour. *Bioact. Mater.* **2020**, *6*, 1107–1117. https://doi.org/10.1016/j.bioactmat.2020.10.001.
17. Capellato, P.; Camargo, S.E.A.; Sachs, D. Biological Response to Nanosurface Modification on Metallic Biomaterials. *Curr. Osteoporos. Rep.* **2020**, *18*, 790–795. https://doi.org/10.1007/s11914-020-00635-x.
18. Wang, K.; Man, K.; Liu, J.; et al. Dissecting Physical and Biochemical Effects in Nanotopographical Regulation of Cell Behavior. *ACS Nano* **2023**, *17*, 2124–2133. https://doi.org/10.1021/acsnano.2c08075.
19. Brammer, K.S.; Frandsen, C.J.; Jin, S. TiO_2 Nanotubes for Bone Regeneration. *Trends Biotechnol.* **2012**, *30*, 315–322. https://doi.org/10.1016/j.tibtech.2012.02.005.
20. Pan, H.; Zhao, J.; Fan, R.; et al. 3D Hierarchically Aligned Nanofiber Scaffolds Promote Cell Migration for Tissue Regeneration. *Nat. Protoc.* **2026**, in press. https://doi.org/10.1038/s41596-026-01339-9.
21. Shi, X.; Xu, C.; Chen, Z.; et al. Biomaterial-Mediated Macrophage Polarization Remodeling and Sequential Regulation: A Potential Strategy in Bone Infections Treatment. *Bone Res.* **2025**, *13*, 96. https://doi.org/10.1038/s41413-025-00471-8.
22. Mooij, I.; Apachitei, I.; Zadpoor, A.A.; et al. Biomaterial Multiscale Geometry for Regenerative Immunoengineering of Bone Tissue. *Acta Biomater.* **2025**, *203*, 21–37. https://doi.org/10.1016/j.actbio.2025.07.036.
23. Tsukasaki, M.; Takayanagi, H. Osteoimmunology: Evolving Concepts in Bone–Immune Interactions in Health and Disease. *Nat. Rev. Immunol.* **2019**, *19*, 626–642. https://doi.org/10.1038/s41577-019-0178-8.
24. Wang, C.; Wu, Q.; Zhuang, L.; et al. Immunometabolism of Macrophages in the Bone Microenvironment: A New Perspective for Bone Healing Therapy. *J. Adv. Res.* **2026**, *82*, 485–506. https://doi.org/10.1016/j.jare.2025.07.046.
25. Yunna, C.; Mengru, H.; Lei, W.; et al. Macrophage M1/M2 Polarization. *Eur. J. Pharmacol.* **2020**, *877*, 173090. https://doi.org/10.1016/j.ejphar.2020.173090.
26. Dai, B.; Zheng, L.; Chung-Wai Cheung, J.; et al. Macrophages: Redefining Extracellular Matrix Architecture through Phenotypic Switches as Therapeutic Targets. *Biomaterials* **2026**, *330*, 124063. https://doi.org/10.1016/j.biomaterials.2026.124063.
27. Hu, K.; Shang, Z.; Yang, X.; et al. Macrophage Polarization and the Regulation of Bone Immunity in Bone Homeostasis. *J. Inflamm. Res.* **2023**, *16*, 3563–3580. https://doi.org/10.2147/JIR.S423819.
28. Yao, Y.; Xu, X.-H.; Jin, L. Macrophage Polarization in Physiological and Pathological Pregnancy. *Front. Immunol.* **2019**, *10*, 792. https://doi.org/10.3389/fimmu.2019.00792.
29. Fernandes, T.L.; Gomoll, A.H.; Lattermann, C.; et al. Macrophage: A Potential Target on Cartilage Regeneration. *Front. Immunol.* **2020**, *11*, 111. https://doi.org/10.3389/fimmu.2020.00111.
30. Toledo, B.; Zhu Chen, L.; Paniagua-Sancho, M.; et al. Deciphering the Performance of Macrophages in Tumour Microenvironment: A Call for Precision Immunotherapy. *J. Hematol. Oncol.* **2024**, *17*, 44. https://doi.org/10.1186/s13045-024-01559-0.
31. Yang, T.; Fang, Z.; Zhang, J.; et al. Physical Cues in Biomaterials Modulate Macrophage Polarization for Bone Regeneration: A Review. *Front. Bioeng. Biotechnol.* **2025**, *13*, 1640560. https://doi.org/10.3389/fbioe.2025.1640560.

32. Halper, J.; Dolfi, B.; Ivanov, S.; et al. Macrophages and Osteoclasts: Similarity and Divergence between Bone Phagocytes. *Front. Immunol.* **2025**, *16*, 1683872. https://doi.org/10.3389/fimmu.2025.1683872.
33. Sun, Y.; Li, J.; Xie, X.; et al. Macrophage-Osteoclast Associations: Origin, Polarization, and Subgroups. *Front. Immunol.* **2021**, *12*, 778078. https://doi.org/10.3389/fimmu.2021.778078.
34. Hu, L.; Liu, R.; Zhang, L. Advance in Bone Destruction Participated by JAK/STAT in Rheumatoid Arthritis and Therapeutic Effect of JAK/STAT Inhibitors. *Int. Immunopharmacol.* **2022**, *111*, 109095. https://doi.org/10.1016/j.intimp.2022.109095.
35. Veis, D.J.; O'Brien, C.A. Osteoclasts, Master Sculptors of Bone. *Annu. Rev. Pathol.* **2023**, *18*, 257–281. https://doi.org/10.1146/annurev-pathmechdis-031521-040919.
36. Arai, F.; Miyamoto, T.; Ohneda, O.; et al. Commitment and Differentiation of Osteoclast Precursor Cells by the Sequential Expression of c-Fms and Receptor Activator of Nuclear Factor κB (RANK) Receptors. *J. Exp. Med.* **1999**, *190*, 1741–1754. https://doi.org/10.1084/jem.190.12.1741.
37. Zha, L.; He, L.; Liang, Y.; et al. TNF-α Contributes to Postmenopausal Osteoporosis by Synergistically Promoting RANKL-Induced Osteoclast Formation. *Biomed. Pharmacother.* **2018**, *102*, 369–374. https://doi.org/10.1016/j.biopha.2018.03.080.
38. Yao, Z.; Getting, S.J.; Locke, I.C. Regulation of TNF-Induced Osteoclast Differentiation. *Cells* **2021**, *11*, 132. https://doi.org/10.3390/cells11010132.
39. Kandahari, A.M.; Yang, X.; Laroche, K.A.; et al. A Review of UHMWPE Wear-Induced Osteolysis: The Role for Early Detection of the Immune Response. *Bone Res.* **2016**, *4*, 16014. https://doi.org/10.1038/boneres.2016.14.
40. Xiao, W.; Shen, Y.; Xu, Y. LOXG473A Induces the Formation of Osteoclasts in RAW264.7 Cells via IL-6/JAK2/STAT3 Signaling. *Exp. Cell Res.* **2021**, *409*, 112890. https://doi.org/10.1016/j.yexcr.2021.112890.
41. Palmqvist, P.; Lundberg, P.; Persson, E.; et al. Inhibition of Hormone and Cytokine-Stimulated Osteoclastogenesis and Bone Resorption by Interleukin-4 and Interleukin-13 Is Associated with Increased Osteoprotegerin and Decreased RANKL and RANK in a STAT6-Dependent Pathway. *J. Biol. Chem.* **2006**, *281*, 2414–2429. https://doi.org/10.1074/jbc.M510160200.
42. Williams, D.F. Biocompatibility Pathways and Mechanisms for Bioactive Materials: The Bioactivity Zone. *Bioact. Mater.* **2021**, *10*, 306–322. https://doi.org/10.1016/j.bioactmat.2021.08.014.
43. Mohamed, S.G.-K.; Sugiyama, E.; Shinoda, K.; et al. Interleukin-10 Inhibits RANKL-Mediated Expression of NFATc1 in Part via Suppression of c-Fos and c-Jun in RAW264.7 Cells and Mouse Bone Marrow Cells. *Bone* **2007**, *41*, 592–602. https://doi.org/10.1016/j.bone.2007.05.016.
44. Chang, M.K.; Raggatt, L.-J.; Alexander, K.A.; et al. Osteal Tissue Macrophages Are Intercalated throughout Human and Mouse Bone Lining Tissues and Regulate Osteoblast Function *in Vitro* and *in Vivo*. *J. Immunol.* **2008**, *181*, 1232–1244. https://doi.org/10.4049/jimmunol.181.2.1232.
45. Pajarinen, J.; Lin, T.; Gibon, E.; et al. Mesenchymal Stem Cell-Macrophage Crosstalk and Bone Healing. *Biomaterials* **2019**, *196*, 80–89. https://doi.org/10.1016/j.biomaterials.2017.12.025.
46. He, Y.; Wang, Y.; Yu, S.; et al. BMP2 Enhance the Osteogenic Effect of BMSCs-Derived Exosomes in Skull Defect of Diabetic Rats. *Mater. Des.* **2024**, *248*, 113517. https://doi.org/10.1016/j.matdes.2024.113517.
47. Song, R.; Yuan, X.; Wan, Z.; et al. Oncostatin-M Functionalized Cryogel Microspheres for Promoting Diabetic Bone Defects Regeneration. *J. Orthop. Transl.* **2025**, *53*, 138–148. https://doi.org/10.1016/j.jot.2025.06.002.
48. Guihard, P.; Danger, Y.; Brounais, B.; et al. Induction of Osteogenesis in Mesenchymal Stem Cells by Activated Monocytes/Macrophages Depends on Oncostatin M Signaling. *Stem Cells* **2012**, *30*, 762–772. https://doi.org/10.1002/stem.1040.
49. Chen, L.; Zhu, J.; Ge, N.; et al. A Biodegradable Magnesium Alloy Promotes Subperiosteal Osteogenesis via Interleukin-10-Dependent Macrophage Immunomodulation. *Biomaterials* **2025**, *318*, 122992. https://doi.org/10.1016/j.biomaterials.2024.122992.
50. Wang, Z.; Lin, M.; Pan, Y.; et al. Periostin^{+} Myeloid Cells Improved Long Bone Regeneration in a Mechanosensitive Manner. *Bone Res.* **2024**, *12*, 59. https://doi.org/10.1038/s41413-024-00361-5.
51. Zhang, J.; Shi, H.; Zhang, N.; et al. Interleukin-4-Loaded Hydrogel Scaffold Regulates Macrophages Polarization to Promote Bone Mesenchymal Stem Cells Osteogenic Differentiation via TGF-β1/Smad Pathway for Repair of Bone Defect. *Cell Prolif.* **2020**, *53*, e12907. https://doi.org/10.1111/cpr.12907.
52. Glass, G.E.; Chan, J.K.; Freidin, A.; et al. TNF-α Promotes Fracture Repair by Augmenting the Recruitment and Differentiation of Muscle-Derived Stromal Cells. *Proc. Natl. Acad. Sci. USA* **2011**, *108*, 1585–1590. https://doi.org/10.1073/pnas.1018501108.
53. Osta, B.; Benedetti, G.; Miossec, P. Classical and Paradoxical Effects of TNF-α on Bone Homeostasis. *Front. Immunol.* **2014**, *5*, 48. https://doi.org/10.3389/fimmu.2014.00048.
54. Jin, C.; Liang, J.; Wu, J.; et al. Temporal Immunomodulatory Hydrogel Regulating the Immune-Osteogenic Cascade for Infected Bone Defects Regeneration. *Adv. Mater.* **2026**, *38*, e14419. https://doi.org/10.1002/adma.202514419.

55. Majrashi, M.; Kotowska, A.; Scurr, D.; et al. Sustained Release of Dexamethasone from 3D-Printed Scaffolds Modulates Macrophage Activation and Enhances Osteogenic Differentiation. *ACS Appl. Mater. Interfaces* **2023**, *15*, 56623–56638. https://doi.org/10.1021/acsami.3c09774.
56. Lu, L.Y.; Loi, F.; Nathan, K.; et al. Pro-Inflammatory M1 Macrophages Promote Osteogenesis by Mesenchymal Stem Cells via the COX-2-Prostaglandin E2 Pathway. *J. Orthop. Res.* **2017**, *35*, 2378–2385. https://doi.org/10.1002/jor.23553.
57. Horwood, N.J. Macrophage Polarization and Bone Formation: A Review. *Clin. Rev. Allergy Immunol.* **2016**, *51*, 79–86. https://doi.org/10.1007/s12016-015-8519-2.
58. Loi, F.; Córdova, L.A.; Zhang, R.; et al. The Effects of Immunomodulation by Macrophage Subsets on Osteogenesis *in Vitro*. *Stem Cell Res. Ther.* **2016**, *7*, 15. https://doi.org/10.1186/s13287-016-0276-5.
59. Zhang, Y.; Shi, J.; Zhu, J.; et al. Immunometabolic Rewiring in Macrophages for Periodontitis Treatment via Nanoquercetin-Mediated Leverage of Glycolysis and OXPHOS. *Acta Pharm. Sin. B* **2024**, *14*, 5026–5036. https://doi.org/10.1016/j.apsb.2024.07.008.
60. Spiller, K.L.; Anfang, R.R.; Spiller, K.J.; et al. The Role of Macrophage Phenotype in Vascularization of Tissue Engineering Scaffolds. *Biomaterials* **2014**, *35*, 4477–4488. https://doi.org/10.1016/j.biomaterials.2014.02.012.
61. Spiller, K.L.; Nassiri, S.; Witherel, C.E.; et al. Sequential Delivery of Immunomodulatory Cytokines to Facilitate the M1-to-M2 Transition of Macrophages and Enhance Vascularization of Bone Scaffolds. *Biomaterials* **2015**, *37*, 194–207. https://doi.org/10.1016/j.biomaterials.2014.10.017.
62. Wu, C.-L.; Harasymowicz, N.S.; Klimak, M.A.; et al. The Role of Macrophages in Osteoarthritis and Cartilage Repair. *Osteoarthritis Cartilage* **2020**, *28*, 544–554. https://doi.org/10.1016/j.joca.2019.12.007.
63. Wynn, T.A.; Vannella, K.M. Macrophages in Tissue Repair, Regeneration, and Fibrosis. *Immunity* **2016**, *44*, 450–462. https://doi.org/10.1016/j.immuni.2016.02.015.
64. Jiang, S.; Li, H.; Zhang, L.; et al. Generic Diagramming Platform (GDP): A Comprehensive Database of High-Quality Biomedical Graphics. *Nucleic Acids Res.* **2025**, *53*, D1670–D1676. https://doi.org/10.1093/nar/gkae973.
65. Asadi Tokmedash, M.; Kim, C.; Chavda, A.P.; et al. Engineering Multifunctional Surface Topography to Regulate Multiple Biological Responses. *Biomaterials* **2025**, *319*, 123136. https://doi.org/10.1016/j.biomaterials.2025.123136.
66. Fox, C.B.; Kim, J.; Schlesinger, E.B.; et al. Fabrication of Micropatterned Polymeric Nanowire Arrays for High-Resolution Reagent Localization and Topographical Cellular Control. *Nano Lett.* **2015**, *15*, 1540–1546. https://doi.org/10.1021/nl503872p.
67. Huang, N.F.; Lai, E.S.; Ribeiro, A.J.S.; et al. Spatial Patterning of Endothelium Modulates Cell Morphology, Adhesiveness and Transcriptional Signature. *Biomaterials* **2013**, *34*, 2928–2937. https://doi.org/10.1016/j.biomaterials.2013.01.017.
68. Biela, S.A.; Su, Y.; Spatz, J.P.; et al. Different Sensitivity of Human Endothelial Cells, Smooth Muscle Cells and Fibroblasts to Topography in the Nano-Micro Range. *Acta Biomater.* **2009**, *5*, 2460–2466. https://doi.org/10.1016/j.actbio.2009.04.003.
69. Wu, Y.; Yue, X.; Zhang, Y.; et al. Dual-Sided Centripetal Microgrooved Poly(D,L-lactide-co-caprolactone) Disk Encased in Immune-Regulating Hydrogels for Enhanced Bone Regeneration. *Mater. Today Bio* **2025**, *30*, 101436. https://doi.org/10.1016/j.mtbio.2024.101436.
70. Joo, S.; Lee, C.-E.; Kang, J.; et al. Intaglio Contact Printing of Versatile Carbon Nanotube Composites and Its Applications for Miniaturizing High-Performance Devices. *Small* **2022**, *18*, 2106174. https://doi.org/10.1002/smll.202106174.
71. Yu, H.; Xu, M.; Xu, W.-C.; et al. Designing Resists for Nanoimprint Lithography Enabling Functional Patterning. *Chin. J. Chem.* **2026**, *44*, 1457–1472. https://doi.org/10.1002/cjoc.70427.
72. Guo, L.J. Nanoimprint Lithography: Methods and Material Requirements. *Adv. Mater.* **2007**, *19*, 495–513. https://doi.org/10.1002/adma.200600882.
73. Sansen, T.; Sanchez-Fuentes, D.; Rathar, R.; et al. Mapping Cell Membrane Organization and Dynamics Using Soft Nanoimprint Lithography. *ACS Appl. Mater. Interfaces* **2020**, *12*, 29000–29012. https://doi.org/10.1021/acsami.0c05432.
74. Lee, T.-Y.; Chen, P.-T.; Huang, C.-C.; et al. Advances in Core Technologies for Semiconductor Manufacturing: Applications and Challenges of Atomic Layer Etching, Neutral Beam Etching and Atomic Layer Deposition. *Nanoscale Adv.* **2025**, *7*, 2796–2817. https://doi.org/10.1039/D4NA00784K.
75. Ariganello, M.B.; Bello, D.G.; Rodriguez-Contreras, A.; et al. Surface Nanocavitation of Titanium Modulates Macrophage Activity. *Int. J. Nanomedicine* **2018**, *13*, 8297–8308. https://doi.org/10.2147/IJN.S185436.
76. Ødegaard, K.S.; Westhrin, M.; Afif, A.B.; et al. The Effects of Surface Treatments on Electron Beam Melted Ti-6Al-4V Disks on Osteogenesis of Human Mesenchymal Stromal Cells. *Biomater. Adv.* **2023**, *147*, 213327. https://doi.org/10.1016/j.bioadv.2023.213327.
77. Hossain, N.; Mobarak, M.H.; Mimona, M.A.; et al. Advances and Significances of Nanoparticles in Semiconductor Applications—A Review. *Results Eng.* **2023**, *19*, 101347. https://doi.org/10.1016/j.rineng.2023.101347.
78. Seong, H.; Higgins, S.G.; Penders, J.; et al. Size-Tunable Nanoneedle Arrays for Influencing Stem Cell Morphology, Gene Expression, and Nuclear Membrane Curvature. *ACS Nano* **2020**, *14*, 5371–5381. https://doi.org/10.1021/acsnano.9b08689.

79. Roy, A.; Patil, D.; Yarlagadda, P.K.D.V.; et al. Cooperative Stiffening of Flexible High Aspect Ratio Nanostructures Impart Mechanobactericidal Activity to Soft Substrates. *J. Colloid Interface Sci.* **2023**, *652*, 2127–2138. https://doi.org/10.1016/j.jcis.2023.09.021.
80. Mahara, A.; Kojima, K.; Yamamoto, M.; et al. Accelerated Tissue Regeneration in Decellularized Vascular Grafts with a Patterned Pore Structure. *J. Mater. Chem. B* **2022**, *10*, 2544–2550. https://doi.org/10.1039/D1TB02271G.
81. Valverde, G.B.; Jimbo, R.; Teixeira, H.S.; et al. Evaluation of Surface Roughness as a Function of Multiple Blasting Processing Variables. *Clin. Oral Implants Res.* **2013**, *24*, 238–242. https://doi.org/10.1111/j.1600-0501.2011.02392.x.
82. Meyerink, J.G.; Kota, D.; Wood, S.T.; et al. Transparent Titanium Dioxide Nanotubes: Processing, Characterization, and Application in Establishing Cellular Response Mechanisms. *Acta Biomater.* **2018**, *79*, 364–374. https://doi.org/10.1016/j.actbio.2018.08.039.
83. Wang, X.; Si, Q.; Yang, N.; et al. TiO_2 Nanotubes Regulate Osteo-Adipogenic Balance through SREBP1 to Determine the Fate of Bone Marrow Mesenchymal Stem Cells. *Regen. Biomater.* **2025**, *12*, rbaf061. https://doi.org/10.1093/rb/rbaf061.
84. Zheng, X.; Chen, L.; Tan, J.; et al. Effect of Micro/Nano-Sheet Array Structures on the Osteo-Immunomodulation of Macrophages. *Regen. Biomater.* **2022**, 9, rbac075. https://doi.org/10.1093/rb/rbac075.
85. Shayan, M.; Padmanabhan, J.; Morris, A.H.; et al. Nanopatterned Bulk Metallic Glass-Based Biomaterials Modulate Macrophage Polarization. *Acta Biomater.* **2018**, *75*, 427–438. https://doi.org/10.1016/j.actbio.2018.05.051.
86. Horii, T.; Tsujimoto, H.; Hagiwara, A.; et al. Effects of Fiber Diameter and Spacing Size of an Artificial Scaffold on the *in Vivo* Cellular Response and Tissue Remodeling. *ACS Appl. Bio Mater.* **2021**, *4*, 6924–6936. https://doi.org/10.1021/acsabm.1c00572.
87. Jiang, S.; Zhou, J.; Zhao, C.; et al. Aligned Electrospun Fibers Inducing Cell and Nuclear Morphology Remodeling via Ras-Associated Protein 1/Yes-Associated Protein Signaling Enhances Bone Regeneration. *Adv. Fiber Mater.* **2025**, *7*, 1980–1997. https://doi.org/10.1007/s42765-025-00596-9.
88. Biomimetic Hydrogel Micro-/Nanofibers for In Situ Soft Tissue Repair and Regeneration. *Bioact. Mater.* **2026**, *55*, 485–502. https://doi.org/10.1016/j.bioactmat.2025.09.035.
89. Zhu, G.; Zhang, R.; Xie, Q.; et al. Shish-Kebab Structure Fiber with Nano and Micro Diameter Regulate Macrophage Polarization for Anti-Inflammatory and Bone Differentiation. *Mater. Today Bio* **2023**, *23*, 100880. https://doi.org/10.1016/j.mtbio.2023.100880.
90. Zhang, X.; Hao, R.; Tong, J.; et al. A Radially Aligned Nanofiber Scaffold with Engineered Guidance Gradients for Directed Cell Migration and Accelerated Wound Healing. *Biomaterials* **2026**, *327*, 123797. https://doi.org/10.1016/j.biomaterials.2025.123797.
91. Asadi Tokmedash, M.; Min, J. Designer Micro-/Nanocrumpled MXene Multilayer Coatings Accelerate Osteogenesis and Regulate Macrophage Polarization. *ACS Appl. Mater. Interfaces* **2024**, *16*, 21415–21426. https://doi.org/10.1021/acsami.3c18158.
92. Ye, Z.; Xu, Z.; Zhang, Y.; et al. Microfluidic Synthesis of Discrete Chiral Gold Nanorods with Tunable Morphologies and Enantioselective Recognition. *ACS Appl. Mater. Interfaces* **2026**, *18*, 4198–4209. https://doi.org/10.1021/acsami.5c21617.
93. Song, J.-N.; Liu, K.; Mei, J.; et al. Defined Surface Physicochemical Cues Inhibit M1 Polarization of Human Macrophages Using Colloidal Self-Assembled Patterns. *ACS Appl. Mater. Interfaces* **2023**, *15*, 35832–35846. https://doi.org/10.1021/acsami.3c04692.
94. Wang, B.; Xiao, S.; Liao, J.; et al. Directional Biomimetic Scaffold-Mediated Cell Migration and Pathological Microenvironment Regulation Accelerate Diabetic Bone Defect Repair. *ACS Nano* **2025**, *19*, 32382–32404. https://doi.org/10.1021/acsnano.5c08238.
95. Wu, B.; Yang, J.; Ye, J.; et al. Extrusion-Based 3D Printing of Cross-Scale Porous Bone Scaffolds and Their Micro-Topological Structures for Bone Repair. *Biomater. Adv.* **2026**, *180*, 214540. https://doi.org/10.1016/j.bioadv.2025.214540.
96. Aboal-Castro, L.; Radziunas-Salinas, Y.; Pita-Vilar, M.; et al. Laser-Assisted Micropatterned 3D Printed Scaffolds with Customizable Surface Topography and Porosity for Modulation of Cell Function. *Adv. Healthc. Mater.* **2025**, *14*, 2403992. https://doi.org/10.1002/adhm.202403992.
97. Li, J.; Jiang, X.; Li, H.; et al. Tailoring Materials for Modulation of Macrophage Fate. *Adv. Mater.* **2021**, *33*, e2004172. https://doi.org/10.1002/adma.202004172.
98. Wang, C.; Chu, C.; Zhao, X.; et al. The Diameter Factor of Aligned Membranes Facilitates Wound Healing by Promoting Epithelialization in an Immune Way. *Bioact. Mater.* **2022**, *11*, 206–217. https://doi.org/10.1016/j.bioactmat.2021.09.022.
99. Dong, X.; Liu, S.; Yang, Y.; et al. Aligned Microfiber-Induced Macrophage Polarization to Guide Schwann-Cell-Enabled Peripheral Nerve Regeneration. *Biomaterials* **2021**, *272*, 120767. https://doi.org/10.1016/j.biomaterials.2021.120767.
100. He, Y.; Zhang, X.; Meng, F.; et al. Biomimetic Chiral Nanotopography for Manipulating Immunological Response. *Adv. Funct. Mater.* **2024**, *34*, 2313157. https://doi.org/10.1002/adfm.202313157.
101. Buskermolen, A.B.C.; Ristori, T.; Mostert, D.; et al. Cellular Contact Guidance Emerges from Gap Avoidance. *Cell Rep. Phys. Sci.* **2020**, *1*, 100055. https://doi.org/10.1016/j.xcrp.2020.100055.

102. Meyle, J.; Gültig, K.; Nisch, W. Variation in Contact Guidance by Human Cells on a Microstructured Surface. *J. Biomed. Mater. Res.* **1995**, *29*, 81–88. https://doi.org/10.1002/jbm.820290112.
103. Wójciak-Stothard, B.; Madeja, Z.; Korohoda, W.; et al. Activation of Macrophage-Like Cells by Multiple Grooved Substrata. Topographical Control of Cell Behaviour. *Cell Biol. Int.* **1995**, *19*, 485–490. https://doi.org/10.1006/cbir.1995.1092.
104. Lee, S.; Choi, J.; Shin, S.; et al. Analysis on Migration and Activation of Live Macrophages on Transparent Flat and Nanostructured Titanium. *Acta Biomater.* **2011**, *7*, 2337–2344. https://doi.org/10.1016/j.actbio.2011.01.006.
105. Mohiuddin, M.; Pan, H.-A.; Hung, Y.-C.; et al. Control of Growth and Inflammatory Response of Macrophages and Foam Cells with Nanotopography. *Nanoscale Res. Lett.* **2012**, *7*, 394. https://doi.org/10.1186/1556-276X-7-394.
106. Dabare, P.R.L.; Bachhuka, A.; Quek, J.Y.; et al. Nano-Roughness-Mediated Macrophage Polarization for Desired Host Immune Response. *Small Sci.* **2023**, *3*, 2300080. https://doi.org/10.1002/smsc.202300080.
107. Necula, M.G.; Mazare, A.; Negrescu, A.M.; et al. Macrophage-Like Cells Are Responsive to Titania Nanotube Intertube Spacing—An *in Vitro* Study. *Int. J. Mol. Sci.* **2022**, *23*, 3558. https://doi.org/10.3390/ijms23073558.
108. Asadi Tokmedash, M.; Robins, J.; VanEpps, J.S.; et al. Multiscale Hybrid Surface Topographies Orchestrate Immune Regulation, Antibacterial Defense, and Tissue Regeneration. *Adv. Healthc. Mater.* **2025**, *14*, e02451. https://doi.org/10.1002/adhm.202502451.
109. Cicuéndez, M.; García-Lizarribar, A.; Casarrubios, L.; et al. Functionality of Macrophages Encapsulated in Porcine Decellularized Adipose Matrix Hydrogels and Interaction with *Candida albicans*. *Biomater. Adv.* **2024**, *159*, 213794. https://doi.org/10.1016/j.bioadv.2024.213794.
110. Singh, S.; Awuah, D.; Rostam, H.M.; et al. Unbiased Analysis of the Impact of Micropatterned Biomaterials on Macrophage Behavior Provides Insights beyond Predefined Polarization States. *ACS Biomater. Sci. Eng.* **2017**, *3*, 969–978. https://doi.org/10.1021/acsbiomaterials.7b00104.
111. Huo, Z.; Yang, W.; Harati, J.; et al. Biomechanics of Macrophages on Disordered Surface Nanotopography. *ACS Appl. Mater. Interfaces* **2024**, *16*, 27164–27176. https://doi.org/10.1021/acsami.4c04330.
112. Changede, R.; Sheetz, M. Integrin and Cadherin Clusters: A Robust Way to Organize Adhesions for Cell Mechanics. *BioEssays* **2017**, *39*, 1–12. https://doi.org/10.1002/bies.201600123.
113. Kanchanawong, P.; Shtengel, G.; Pasapera, A.M.; et al. Nanoscale Architecture of Integrin-Based Cell Adhesions. *Nature* **2010**, *468*, 580–584. https://doi.org/10.1038/nature09621.
114. Oh, S.; Brammer, K.S.; Li, Y.S.J.; et al. Stem Cell Fate Dictated Solely by Altered Nanotube Dimension. *Proc. Natl. Acad. Sci. USA* **2009**, *106*, 2130–2135. https://doi.org/10.1073/pnas.0813200106.
115. Xu, W.-C.; Dong, X.; Ding, J.-L.; et al. Nanotubular TiO_2 Regulates Macrophage M2 Polarization and Increases Macrophage Secretion of VEGF to Accelerate Endothelialization via the ERK1/2 and PI3K/AKT Pathways. *Int. J. Nanomedicine* **2019**, *14*, 441–455. https://doi.org/10.2147/IJN.S188439.
116. Li, K.; Lv, L.; Shao, D.; et al. Engineering Nanopatterned Structures to Orchestrate Macrophage Phenotype by Cell Shape. *J. Funct. Biomater.* **2022**, *13*, 31. https://doi.org/10.3390/jfb13010031.
117. Luu, T.U.; Gott, S.C.; Woo, B.W.; et al. Micro- and Nanopatterned Topographical Cues for Regulating Macrophage Cell Shape and Phenotype. *ACS Appl. Mater. Interfaces* **2015**, *7*, 28665–28672. https://doi.org/10.1021/acsami.5b10589.
118. Xie, J.; Wu, X.; Zheng, S.; et al. Aligned Electrospun Poly(L-lactide) Nanofibers Facilitate Wound Healing by Inhibiting Macrophage M1 Polarization via the JAK-STAT and NF-κB Pathways. *J. Nanobiotechnology* **2022**, *20*, 342. https://doi.org/10.1186/s12951-022-01549-9.
119. Hao, J.; Du, L.; He, Y.; et al. Bioceramic Surface Topography Regulating Immune Osteogenesis. *BME Front.* **2025**, *6*, 0089. https://doi.org/10.34133/bmef.0089.
120. Wu, J.; Feng, C.; Wang, M.; et al. Whisker of Biphasic Calcium Phosphate Ceramics: Osteo-Immunomodulatory Behaviors. *Nano Res.* **2022**, *15*, 9169–9182. https://doi.org/10.1007/s12274-022-4591-0.
121. Tylek, T.; Blum, C.; Hrynevich, A.; et al. Precisely Defined Fiber Scaffolds with 40 µm Porosity Induce Elongation Driven M2-Like Polarization of Human Macrophages. *Biofabrication* **2020**, *12*, 025007. https://doi.org/10.1088/1758-5090/ab5f4e.
122. Vassey, M.J.; Figueredo, G.P.; Scurr, D.J.; et al. Immune Modulation by Design: Using Topography to Control Human Monocyte Attachment and Macrophage Differentiation. *Adv. Sci.* **2020**, *7*, 1903392. https://doi.org/10.1002/advs.201903392.
123. Hang, R.; Zhao, Y.; Zhang, Y.; et al. The Role of Nanopores Constructed on the Micropitted Titanium Surface in the Immune Responses of Macrophages and the Potential Mechanisms. *J. Mater. Chem. B* **2022**, *10*, 7732–7743. https://doi.org/10.1039/D2TB01263D.
124. Jin, S.; Wen, J.; Zhang, Y.; et al. M2 Macrophage-Derived Exosome-Functionalized Topological Scaffolds Regulate the Foreign Body Response and the Coupling of Angio/Osteoclasto/Osteogenesis. *Acta Biomater.* **2024**, *177*, 91–106. https://doi.org/10.1016/j.actbio.2024.01.043.
125. Yang, Y.; Lin, Y.; Zhang, Z.; et al. Micro/Nano-Net Guides M2-Pattern Macrophage Cytoskeleton Distribution via Src–ROCK Signalling for Enhanced Angiogenesis. *Biomater. Sci.* **2021**, *9*, 3334–3347. https://doi.org/10.1039/D1BM00116G.

126. Jin, S.; Yang, R.; Chu, C.; et al. Topological Structure of Electrospun Membrane Regulates Immune Response, Angiogenesis and Bone Regeneration. *Acta Biomater.* **2021**, *129*, 148–158. https://doi.org/10.1016/j.actbio.2021.05.042.
127. Narayanan, K.B. Nanotopographical Features of Polymeric Nanocomposite Scaffolds for Tissue Engineering and Regenerative Medicine: A Review. *Biomimetics* **2025**, *10*, 317. https://doi.org/10.3390/biomimetics10050317.
128. Liliensiek, S.J.; Nealey, P.; Murphy, C.J. Characterization of Endothelial Basement Membrane Nanotopography in Rhesus Macaque as a Guide for Vessel Tissue Engineering. *Tissue Eng. Part A* **2009**, *15*, 2643–2651. https://doi.org/10.1089/ten.tea.2008.0284.
129. Qiao, W.; Xie, H.; Fang, J.; et al. Sequential Activation of Heterogeneous Macrophage Phenotypes Is Essential for Biomaterials-Induced Bone Regeneration. *Biomaterials* **2021**, *276*, 121038. https://doi.org/10.1016/j.biomaterials.2021.121038.
130. Shen, X.; Yu, Y.; Ma, P.; et al. Titania Nanotubes Promote Osteogenesis via Mediating Crosstalk between Macrophages and MSCs under Oxidative Stress. *Colloids Surf. B Biointerfaces* **2019**, *180*, 39–48. https://doi.org/10.1016/j.colsurfb.2019.04.033.
131. Yin, Y.; He, X.-T.; Wang, J.; et al. Pore Size-Mediated Macrophage M1-to-M2 Transition Influences New Vessel Formation within the Compartment of a Scaffold. *Appl. Mater. Today* **2020**, *18*, 100466. https://doi.org/10.1016/j.apmt.2019.100466.
132. Hong, H.; Lee, S.; Kang, C.; et al. Tuning Liganded Nanocrack Geometry for Dynamic Regulation of Host Macrophages. *Chem. Eng. J.* **2025**, *521*, 166414. https://doi.org/10.1016/j.cej.2025.166414.
133. Dahri, M.; Rezaeian, M.; Sadeghzadeh, H.; et al. Nanomaterial-Driven Macrophage Polarization: Emerging Strategies for Immunomodulation and Regenerative Medicine. *Biomed. Pharmacother.* **2025**, *190*, 118360. https://doi.org/10.1016/j.biopha.2025.118360.
134. Wang, J.; Meng, F.; Song, W.; et al. Nanostructured Titanium Regulates Osseointegration via Influencing Macrophage Polarization in the Osteogenic Environment. *Int. J. Nanomedicine* **2018**, *13*, 4029–4043. https://doi.org/10.2147/IJN.S163956.
135. Tao, B.; Lan, H.; Zhou, X.; et al. Regulation of TiO_2 Nanotubes on Titanium Implants to Orchestrate Osteo/Angio-Genesis and Osteo-Immunomodulation for Boosted Osseointegration. *Mater. Des.* **2023**, *233*, 112268. https://doi.org/10.1016/j.matdes.2023.112268.
136. Guo, M.; Li, T.; Zhang, W.-C.; et al. Wetting of Cell Aggregates on Microdisk Topography Structures Achieved by Maskless Optical Projection Lithography. *Small* **2023**, *19*, e2300311. https://doi.org/10.1002/smll.202300311.
137. Mei, F.; Guo, Y.; Wang, Y.; et al. Matrix Stiffness Regulates Macrophage Polarisation via the Piezo1-YAP Signalling Axis. *Cell Prolif.* **2024**, *57*, e13640. https://doi.org/10.1111/cpr.13640.
138. Chen, L.; Yao, Z.; Zhang, S.; et al. Biomaterial-Induced Macrophage Polarization for Bone Regeneration. *Chin. Chem. Lett.* **2023**, *34*, 107925. https://doi.org/10.1016/j.cclet.2022.107925.
139. Saino, E.; Focarete, M.L.; Gualandi, C.; et al. Effect of Electrospun Fiber Diameter and Alignment on Macrophage Activation and Secretion of Proinflammatory Cytokines and Chemokines. *Biomacromolecules* **2011**, *12*, 1900–1911. https://doi.org/10.1021/bm200248h.
140. Sun, Z.; Guo, S.S.; Fässler, R. Integrin-Mediated Mechanotransduction. *J. Cell Biol.* **2016**, *215*, 445–456. https://doi.org/10.1083/jcb.201609037.
141. Legerstee, K.; Houtsmuller, A.B. A Layered View on Focal Adhesions. *Biology* **2021**, *10*, 1189. https://doi.org/10.3390/biology10111189.
142. Atcha, H.; Jairaman, A.; Holt, J.R.; et al. Mechanically Activated Ion Channel Piezo1 Modulates Macrophage Polarization and Stiffness Sensing. *Nat. Commun.* **2021**, *12*, 3256. https://doi.org/10.1038/s41467-021-23482-5.
143. Linder, S.; Wiesner, C. Tools of the Trade: Podosomes as Multipurpose Organelles of Monocytic Cells. *Cell. Mol. Life Sci.* **2014**, *72*, 121–135. https://doi.org/10.1007/s00018-014-1731-z.
144. Lukácsi, S.; Nagy-Baló, Z.; Erdei, A.; et al. The Role of CR3 (CD11b/CD18) and CR4 (CD11c/CD18) in Complement-Mediated Phagocytosis and Podosome Formation by Human Phagocytes. *Immunol. Lett.* **2017**, *189*, 64–72. https://doi.org/10.1016/j.imlet.2017.05.014.
145. Sosa, B.A.; Rothballer, A.; Kutay, U.; et al. LINC Complexes Form by Binding of Three KASH Peptides to Domain Interfaces of Trimeric SUN Proteins. *Cell* **2012**, *149*, 1035–1047. https://doi.org/10.1016/j.cell.2012.03.046.
146. Jain, N.; Vogel, V. Spatial Confinement Downsizes the Inflammatory Response of Macrophages. *Nat. Mater.* **2018**, *17*, 1134–1144. https://doi.org/10.1038/s41563-018-0190-6.
147. Jia, H.; Zhang, H.; Mo, D.; et al. UTX Responds to Nanotopography to Suppress Macrophage Inflammatory Response by Remodeling H3K27me3 Modification. *Adv. Sci.* **2025**, *12*, e2505723. https://doi.org/10.1002/advs.202505723.
148. Wang, H.; Yu, H.; Huang, T.; et al. Hippo-YAP/TAZ Signaling in Osteogenesis and Macrophage Polarization: Therapeutic Implications in Bone Defect Repair. *Genes Dis.* **2023**, *10*, 2528–2539. https://doi.org/10.1016/j.gendis.2022.12.012.
149. Wei, Q.; Du, F.; Cui, J.; et al. Non-Monotonic Response of Macrophages to Mechanical Stretch Impacts Skin Wound Healing. *Cell. Mol. Biol. Lett.* **2025**, *30*, 82. https://doi.org/10.1186/s11658-025-00764-0.
150. Dupont, S.; Morsut, L.; Aragona, M.; et al. Role of YAP/TAZ in Mechanotransduction. *Nature* **2011**, *474*, 179–183. https://doi.org/10.1038/nature10137.

151. Fu, Y.; Jing, Z.; Chen, T.; et al. Nanotube Patterning Reduces Macrophage Inflammatory Response via Nuclear Mechanotransduction. *J. Nanobiotechnology* **2023**, *21*, 229. https://doi.org/10.1186/s12951-023-01912-4.
152. Hou, Y.; Conklin, B.; Choi, H.K.; et al. Probing Nanotopography-Mediated Macrophage Polarization via Integrated Machine Learning and Combinatorial Biophysical Cue Mapping. *ACS Nano* **2024**, *18*, 25465–25477. https://doi.org/10.1021/acsnano.4c04406.
153. Carrara, S.C.; Davila-Lezama, A.; Cabriel, C.; et al. 3D Topographies Promote Macrophage M2d-Subset Differentiation. *Mater. Today Bio* **2024**, *24*, 100897. https://doi.org/10.1016/j.mtbio.2023.100897.
154. Ivanova, E.P.; Hasan, J.; Webb, H.K.; et al. Natural Bactericidal Surfaces: Mechanical Rupture of *Pseudomonas aeruginosa* Cells by Cicada Wings. *Small* **2012**, *8*, 2489–2494. https://doi.org/10.1002/smll.201200528.
155. Watson, G.S.; Green, D.W.; Schwarzkopf, L.; et al. A Gecko Skin Micro/Nano Structure—A Low Adhesion, Superhydrophobic, Anti-Wetting, Self-Cleaning, Biocompatible, Antibacterial Surface. *Acta Biomater.* **2015**, *21*, 109–122. https://doi.org/10.1016/j.actbio.2015.03.007.
156. Ivanova, E.P.; Linklater, D.P.; Werner, M.; et al. The Multi-Faceted Mechano-Bactericidal Mechanism of Nanostructured Surfaces. *Proc. Natl. Acad. Sci. USA* **2020**, *117*, 12598–12605. https://doi.org/10.1073/pnas.1916680117.
157. Lin, N.; Berton, P.; Moraes, C.; et al. Nanodarts, Nanoblades, and Nanospikes: Mechano-Bactericidal Nanostructures and Where to Find Them. *Adv. Colloid Interface Sci.* **2018**, *252*, 55–68. https://doi.org/10.1016/j.cis.2017.12.007.
158. Finbloom, J.A.; Huynh, C.; Huang, X.; et al. Bioinspired Nanotopographical Design of Drug Delivery Systems. *Nat. Rev. Bioeng.* **2023**, *1*, 139–152. https://doi.org/10.1038/s44222-022-00010-8.
159. del Campo, A.; Arzt, E. Fabrication Approaches for Generating Complex Micro− and Nanopatterns on Polymeric Surfaces. *Chem. Rev.* **2008**, *108*, 911–945. https://doi.org/10.1021/cr050018y.
160. Woodruff, M.A.; Hutmacher, D.W. The Return of a Forgotten Polymer—Polycaprolactone in the 21st Century. *Prog. Polym. Sci.* **2010**, *35*, 1217–1256. https://doi.org/10.1016/j.progpolymsci.2010.04.002.
161. Pandey, S.; Bednarz, P.; Veiseh, O. Tuning Biomaterial Surfaces to Modulate Host-Immune Reactions. *Langmuir* **2025**, *41*, 17355–17368. https://doi.org/10.1021/acs.langmuir.5c01344.
162. Camarero-Espinosa, S.; Carlos-Oliveira, M.; Liu, H.; et al. 3D Printed Dual-Porosity Scaffolds: The Combined Effect of Stiffness and Porosity in the Modulation of Macrophage Polarization. *Adv. Healthc. Mater.* **2022**, *11*, 2101415. https://doi.org/10.1002/adhm.202101415.
163. Hamraoui, A. Cell Adhesion and Surface Interactions: A Comprehensive Review of Surface Energy, Wettability, and Topography Effects. *AIP Adv.* **2025**, *15*, 090702. https://doi.org/10.1063/5.0280399.
164. Chen, Z.; Bachhuka, A.; Han, S.; et al. Tuning Chemistry and Topography of Nanoengineered Surfaces to Manipulate Immune Response for Bone Regeneration Applications. *ACS Nano* **2017**, *11*, 4494–4506. https://doi.org/10.1021/acsnano.6b07808.